Title: High-resolution age modelling of peat bogs from northern Alberta, Canada, using pre- and post-bomb ^{14}C, ^{210}Pb and historical cryptotephra

Author names and affiliations: Lauren J. Davies[1], Peter Appleby[2], Simon van Bellen[3,4], Britta J.L. Jensen[1], Gabriel Magnan[3,4], Gillian Mullan-Boudreau[4], Tommy Noernberg[4], Bob Shannon[5], William Shotyk[4], Claudio Zaccone[6], Duane G. Froese[1]

[1] Department of Earth and Atmospheric Sciences, University of Alberta, Edmonton, AB, T6G 2E3, Canada
[2] Department of Mathematical Sciences, University of Liverpool, Liverpool, L69 3BX, United Kingdom
[3] Geotop, Université du Québec à Montréal, Montréal, QC, H3C 3P8, Canada
[4] Department of Renewable Resources, University of Alberta, Edmonton, AB, T6G 2H1, Canada
[5] Quality Radioanalytical Support, LLC, Grand Marais, Minnesota, 55604, United States
[6] Department of the Sciences of Agriculture, Food and Environment, University of Foggia, 71122 Foggia, Italy

Corresponding author: Lauren J. Davies, ljdavies@ualberta.ca

Abstract: High-resolution studies of peat profiles are frequently undertaken to investigate natural and anthropogenic disturbances over time. However, overlapping profiles of the most commonly applied age-dating techniques, including ^{14}C and ^{210}Pb, often show significant offsets (>decadal) and biases that can be difficult to resolve. Here we investigate variations in the chronometers and individual site histories from six ombrotrophic peat bogs in central and northern Alberta. Dates produced using pre- and post-bomb ^{14}C, ^{210}Pb (corroborated with ^{137}Cs and ^{241}Am), and cryptotephra peaks, are compared and then integrated using OxCal's *P_Sequence* function to produce a single Bayesian age model. Environmental histories for each site obtained using physical and chemical characteristics of the peat cores, e.g. macrofossils, humification, ash content, and dry density, provide important constraints for the models by highlighting periods with significant changes in accumulation rate, e.g. fire events, permafrost development, and prolonged surficial drying. Despite variable environmental histories, it is possible to produce high-resolution age-depth models for each core sequence. Consistent offsets between ^{14}C and ^{210}Pb dates pre-1960s are seen at five of the six sites, but tephra-corrected ^{210}Pb data can be used to produce more coherent models at three of these sites. Processes such as permafrost development and thaw, surficial drying and local fires can disrupt the normal processes by which chronological markers and environmental records are incorporated in the peat record. In consequence, applying standard dating methodologies to these records will result in even greater uncertainties and discrepancies between the different dating tools. These results show that using any single method to accurately date peat profiles where accumulation has not been uniform over time may be unreliable, but a comprehensive multi-method investigation paired with the application of Bayesian statistics can produce more robust chronologies. New cryptotephra data for the Alberta region are also reported here, including the historical Novarupta-Katmai 1912 eruption, White River Ash (East), and glass from Mt. St. Helens, Mt. Churchill, and probable Aleutian sources.

Keywords (<6): Peat, chronology, Anthropocene, Bayesian age modelling

1. Introduction

Holocene peat records preserve abundant organic material and small amounts of other constituents that can record both natural and anthropogenic disturbances over time (e.g. Barber, 1993; Blackford, 2000; Charman et al., 2001; Zhao et al., 2007; Swindles et al., 2012). Ombrotrophic bogs – peatlands that receive water and nutrients almost exclusively from precipitation - are commonly studied as they predominantly receive inputs by atmospheric deposition and can be exceptional archives of past environmental change (Charman et al., 2009; Booth et al., 2010). These archives retain atmospheric inputs, such as particulate matter, and preserve a chronological record of their deposition. Records of particular interest include pollutants (e.g. PCBs and PAHs - Bracewell et al., 1993; Berset et al., 2001; Dreyer et al., 2005; Zaccone et al., 2009; Bao et al., 2014; major and trace metals – Shotyk et al., 1992, 1996; Martínez and McBride, 1999; Roos-Barraclough et al., 2002; Zaccone et al., 2008; de Vleeschouwer et al., 2009; proxies for fossil fuel combustion - Oldfield et al., 1981) and atmospheric dusts (e.g. Sapkota et al., 2007; Le Roux et al., 2012; Fiałkiewicz-Kozieł et al., 2016). To interpret palaeoenvironmental records from peatlands, however, an understanding of both the external forcing and internal processes is required (Barber and Charman, 2014).

When considering the modern period, dating peat can be difficult due to the signals being studied occurring within the acrotelm – the living section of a peat bog with relatively loose material, large pore spaces, and periodic saturation by water. The acrotelm has high permeability and rates of decomposition compared to the catotelm, which is permanently saturated, commonly dense, compressed peat with low permeability. This simple two-dimensional model has been widely used to understand peat hydrology and ecology, modelling and nutrient budgeting since the 1970s (e.g.

Ingram, 1978), and the boundary between the two 'layers' in a peatland varies over time based on the water table depth. While the depth of this boundary is also different between, and potentially within, peatlands, recent anthropogenic influences or climatic anomalies such as the Little Ice Age will be recorded at adjacent depths. These records, therefore, will be affected by changes in signal preservation and taphonomic processes (e.g. transportation, burial, and decomposition) across the boundary. While high peat accumulation rates and increased precision of analytical techniques may imply certain resolutions are obtainable (e.g. annual, seasonal), such variable taphonomic influences and subsequent preservation of the different proxies within the peat sequence will likely increase the observed signal noise and place a limit on interpretation.

Due to variable rates of peat accumulation and decomposition, the interpretation of age-depth relationships in peat archives can be complex and subject to uncertainty (e.g. Belyea and Warner, 1994); at the same time, without reliable chronological control, the records they preserve are of limited use. Several chronological approaches are commonly applied to dating peat sequences, including radiocarbon (^{14}C; e.g. Piotrowska et al., 2011) and lead dating (^{210}Pb; e.g. Appleby et al., 1988; Le Roux and Marshall, 2011). Chronostratigraphic markers such as fallout isotopes, pollen markers, spheroidal carbonaceous particles (SCPs), and cryptotephra can also provide additional information (e.g. Barber et al., 1998; Yang et al., 2001; Swindles et al., 2010; van der Plicht et al., 2013). Turetsky et al. (2004) provide a review of these techniques, but there has been little consensus in the literature on which approach is best. This relates in part to the variable nature of peatlands – small-scale features such as hummocks, hollows, pools, and lawns typically vary in length (Baird et al., 2009) and can have different plant communities, biogeochemical behaviour, and water table

characteristics (Belyea and Clymo, 2001). Relatively short-term disturbances such as fires and surface peat burning, permafrost development and degradation, or the preservation of relict features, do not necessarily have uniform effects on a peatland or reflect systems in equilibrium (e.g. Halsey et al., 1995). The combination of these factors causes inherent variability in peat profiles.

Peat is composed primarily of organic matter and is therefore well suited for ^{14}C dating, although the type of material available may change through a sequence due to shifts in the plant communities present or the degree of decomposition. High-resolution age models have been produced from studies using both pre- and post-bomb ^{14}C dates or wiggle-matching techniques (van Geel and Mook, 1989; Blaauw et al., 2004; Goslar et al., 2005; van der Linden et al., 2008). Different chemical and particulate fractions may produce different ages, and bulk dates may differ from individually picked plant macrofossils (e.g. Chambers et al., 1979; Kilian et al., 1995; Shore et al., 1995; Nilsson et al., 2001; Blaauw et al., 2003; Charman and Garnett, 2005; Brock et al., 2011; Holmquist et al., 2016).

^{210}Pb dating is commonly applied to modern records (e.g. Clymo et al., 1990; Appleby et al., 1997; MacKenzie et al., 1997; Le Roux and Marshall, 2011; Sanchez-Cabeza and Ruiz-Fernández, 2012), and requires corroboration from independent chronostratigraphic markers (Oldfield et al., 1995). A common criticism of ^{210}Pb dating is the potential for mobilisation of ^{210}Pb and other associated chronological markers (e.g. ^{137}Cs) within peat sequences (e.g. Urban et al., 1990; Sanders et al., 1995; Ali et al., 2008; Parry et al., 2013). This has been disputed experimentally (e.g. Vile et al., 1999) and studies have shown good agreement between ^{210}Pb ages and other chronometers (e.g. El-Daoushy et al., 1982; Wieder et al., 1994; MacKenzie et al., 1997; Shotyk et al., 1997). Attempts to combine overlapping ^{14}C and ^{210}Pb dates

have had mixed success – in some instances bomb-peak ^{14}C dates match ^{210}Pb dates well (e.g. Roos-Barraclough and Shotyk, 2003; Le Roux et al., 2005; Rausch et al., 2005), while in others significant offsets are present between the two methods, particularly further back in time (e.g. Goodsite et al., 2001; Bauer et al., 2009; Piotrowska et al., 2010; van der Plicht et al., 2013; Fiałkiewicz-Kozieł et al., 2015).

Records of cryptotephra - non-visible horizons of volcanic ash from distal sources- are well established in peatlands globally (e.g. Dugmore et al., 1996; Lowe et al., 2013; Mackay et al., 2016; Payne et al., 2008; Pyne-O'Donnell et al., 2012; Zaretskaia et al., 2001) and are a useful chronostratigraphic tool (Pilcher et al., 1995; Plunkett, 2006; Swindles et al., 2010). If correlations can be made with well-dated tephra (e.g. historical eruptions, or tephra preserved within annually resolved records) then these tightly constrained ages can be included in age-depth models (e.g. Schoning et al., 2005) and used as an independent test of other chronological methods applied to the same material (e.g. Oldfield et al., 1997). Ombrotrophic peatlands downwind of active volcanic sources are ideal traps for cryptotephra as they can preserve more cryptotephra layers than nearby lakes (Watson et al., 2016) and are thought to be subject to less reworking within a stratigraphic sequence than lacustrine or marine records (Beierle and Bond, 2002; Clymo and Mackay, 1987; Griggs et al., 2015; Payne et al., 2005; Pyne-O'Donnell, 2011). However, the potential close history between peatlands and human activity (e.g. human and animal traffic, peat removal for fuel) means anthropogenic effects must be considered (Swindles et al., 2013). There is also no guarantee that ash from a given eruption will be preserved in identifiable concentrations, and where it is preserved, layers may be discontinuous (e.g. Bergman et al., 2004; Payne and Gehrels, 2010; Zoltai, 1989) or re-deposited after the initial eruption (Davies et al., 2007). Variation is common between records

preserved within a local area or a given peatland due to the interaction of regional and local factors affecting deposition and preservation (Watson et al., 2015).

Here, we compare three different techniques commonly applied to dating peat sequences (accelerator mass spectrometry - ^{14}C; gamma spectrometry - ^{210}Pb, ^{137}Cs and ^{241}Am; and cryptotephra) and combine and model the results using Bayesian statistics. Bayesian statistical techniques have been utilised in a wide range of fields to produce detailed age-depth models based on a relatively small number of dates (e.g. Christen et al., 1995; Litton and Buck, 1995). Bayesian models, through their inclusion of additional (prior) information, provide more precise interpolations than using raw dates alone (e.g. Blaauw and Christen, 2005; Bronk Ramsey, 2008) and provide additional benefits for identifying outliers or anomalous circumstances in the archived sequences (e.g. hiatuses, reversals).

The combination of multiple chronometers and sediment accumulation rates has been used to highlight differences between chronological methods and produce a more accurate final age-model in lacustrine sediments (Tylmann et al., 2016). Additional supporting environmental data preserved within peat cores can also be used as additional model input to constrain peat accumulation. Changes in plant macrofossil composition can affect peat accumulation rates (e.g. Yeloff et al., 2006), and stratigraphic units relating to records of local fires, permafrost development, shifts in the dominant plant species present, peat humification, etc, can therefore be defined and linked to abrupt changes in peat archives.

The peatlands of western interior Canada have been extensively studied over both modern and Holocene timescales (e.g. Beilman et al., 2001; Campbell et al., 2000; Turetsky et al., 2007; Vitt et al., 1994; Yu et al., 2003; Zoltai and Vitt, 1990). We focus on the Fort McMurray region here as the study of local and regional

atmospheric trace elements and organic compounds (e.g. Shotyk et al., 2017, 2016; Zhang et al., 2016) require chronological accuracy and precision on a sub-centennial, and ideally sub-decadal timescale.

Alberta is also downwind of many active volcanoes (Alaska Volcano Observatory; Miller et al., 1998) and has well-established records of visible tephra (e.g. Clague et al., 1995; Jensen and Beaudoin, 2016; Kuehn et al., 2009; Osborn, 1985; Westgate et al., 1970, 1969; Zoltai, 1989). It is likely that tephra can be used to constrain the age models (as their associated errors are smaller than those produced with other methods, e.g. ^{14}C) and to highlight and help to interpret any potential differences in the other chronometers. Key potential tephra here are modern eruptions from sources in Alaska (Davies et al., 2016) or the regionally widespread eastern lobe of the White River Ash (WRAe; Péwé, 1975) that has precise associated ages from wiggle matching of buried tree stumps and Greenland ice core chronologies (Coulter et al., 2012; Jensen et al., 2014; Toohey and Sigl, 2017).

Here we report data from six ombrotrophic peatlands in Alberta, Canada. Multiple peat sequences allow us to assess regional variation by determining how well the chronometers are represented at each site, if there are observable patterns when comparing methods and if our approach for combining and modelling the chronometers using Bayesian statistics is successful across a variety of cores and locations.

2. Regional setting

Cores were collected from six peatlands within the boreal plains of northern Alberta in the summers of 2013 and 2014: five from the Fort McMurray area (Anzac, ANZ; McKay, McK; McMurray, McM; Mildred, MIL; and Jack Pine Hills, JPH-4) and one

from a bog located north of Utikuma Lake (UTK) (Figure 1). Both areas have an estimated 10-30% peatland surface cover with typical depths of 2.5-4.0 m (Vitt et al., 2000).

Fort McMurray is located in north-eastern Alberta and has a dry boreal climate with average daily temperatures ranging from -17°C in January to +17°C in July (1981-2010 data; Environment and Climate Change Canada, 2017). It lies within the zone of sporadic permafrost (Zoltai, 1995; Beilman et al., 2001) and receives ~420 mm average annual precipitation, mainly falling in the summer months (1981-2010 data; Environment and Climate Change Canada, 2017).

UTK is located in north-central Alberta, ~260 km southwest of the Fort McMurray sites. This is within the Utikuma Region Study Area (URSA) that has been a focus of long-term studies of peatland hydrology and biogeochemistry in Alberta (Devito et al., 2012, 2016; Petrone et al., 2016). It has a boreal climate with average daily temperatures ranging from -14°C in January to +15°C in July (1971-2000 data for Slave Lake; Environment and Climate Change Canada, 2017). The region is located outside the present-day southern limit of permafrost distribution and has relatively higher average annual precipitation (~500 mm) than the Fort McMurray area, which is also focused in the summer months.

3. Material and methods

The cores used within this study have been previously discussed by other collaborative investigations (e.g. Mullan-Boudreau et al., 2017; Shotyk et al., 2017, 2016; Zhang et al., 2016; Magnan et al., 2018; van Bellen et al., 2018). The subsampling protocol for the peat samples is detailed in Appendix A. A flow diagram outlining the steps taken to produce the final age models here is included in the

Supplementary Information (Figure S1). Information regarding the environmental histories, three independent chronometers, and resulting Bayesian models is outlined in the subsections below.

3.1 Environmental histories

Supporting data produced from the cores were used to identify potential significant changes in peat accumulation or preservation. Proxies used include plant macrofossils including macroscopic charcoal and charred plant remains (Magnan et al., 2018), testate amoeba assemblages (van Bellen et al., 2018), measurements of dry density, pH, ash content (Mullan-Boudreau et al., 2017), and the degree of peat humification, evaluated using the main atomic ratios (C:N, H:C, O:C) in conjunction with stable isotope analyses ($\delta^{13}C$ and $\delta^{15}N$). When considered together, these data highlight periods of environmental importance such as permafrost development and/or degradation (i.e. drier bog surface and the establishment of xerophilous vegetation); local fires from peaks of macroscopic charcoal >1 mm and charred plant macrofossils; changes in surface wetness from testate amoeba assemblages, moss species, and increased presence of *Picea* needles; and peatland succession (e.g. fen-bog transitions shown with changes in dominant bryophytes, decreasing ash content and pH). At the depths of these changes additional information can be used as input for the age-depth models to more accurately represent the preserved records (see *Section 3.4* for details).

Five of these sites have been ombrotrophic for the entire period covered by the cores collected; MIL has a shallow ombrotrophic zone near the surface and was minerotrophic preceding this (Mullan-Boudreau et al., 2017).

3.2 Cryptotephra analysis

No visible tephra were identified in any of the peat cores. Targeted cryptotephra analyses were undertaken using contiguous 1 cm subsamples from the uppermost sections of the cores (to identify modern ash-fall events) and using every other cm for a targeted 20-30 cm period near the base of the cores (to identify WRAe). The depths to be analysed were determined using ^{14}C dates from the modern day back to ~AD 1850 and for up to 800 years surrounding the AD 853 eruption of WRAe.

Standard methods were used to produce glass shard concentration profiles (Blockley et al., 2005) and the heavy liquid Lithium Heteropolytungstate (LST) was used for density separations. Glass shards for geochemical analysis were re-extracted from peaks in shard concentration using acid digestion (Dugmore et al., 1995), which has been shown to efficiently remove peat fibres without chemically altering or degrading the glass shards (Roland et al., 2015). Samples were mounted in an epoxy puck and polished to expose glass surfaces before being carbon coated prior to electron probe microanalysis (EPMA). New data are reported here from glass shards analysed on a JEOL 8900 Superprobe and Cameca SX100 at the University of Alberta by wavelength dispersive X-ray spectroscopy (WDS) following established protocols (e.g. Jensen et al., 2008).

A standard suite of ten elements (Si, Ti, Al, Fe, Mn, Mg, Ca, Na, K, Cl) were measured using a 5 μm beam with 15 keV accelerating voltage and 6 nA beam current to minimise alkali migration during analyses (Spray and Rae, 1995; Morgan and London, 2005). Where intensity data loss does occur, it has been shown that empirical corrections can be applied if the data demonstrate linear variance over time (Nielsen and Sigurdsson, 1981). Here both Si and Na were corrected for Time Dependent Intensity (TDI) loss (or gain) using a self-calibrated correction with Probe for EPMA software (Donovan et al., 2015).

Two secondary standards of known composition were run concurrently with all tephra samples: ID 3506, a Lipari rhyolite obsidian, and a reference sample of Old Crow tephra, a well-characterized, secondarily hydrated tephra bed (e.g. Kuehn et al., 2011). All results were normalized to 100% and presented as weight percent (wt%) oxides. New major-element geochemical data and associated standard measurements, as well data points for relevant reference material, are reported in the Supplementary Information (Table S1).

3.3 Radiometric dating

3.3.1 ^{14}C dating

A total of 63 pre- and post-bomb ^{14}C dates were produced for the six cores (representing nine to eleven dates per core) from identified plant macrofossils. *Sphagnum* remains were preferred where possible as they yield the most reliable ^{14}C dates (Nilsson et al., 2001), however other terrestrial plant macrofossils (e.g. twigs, needles, leaves, seeds) were used in some samples to provide sufficient mass for analysis.

All ^{14}C samples were pre-treated at the University of Alberta following standard procedures (e.g. Reyes et al., 2010) and analysed at the Keck-Carbon Cycle AMS facility (University of California, Irvine). Two secondary standards were also pre-treated concurrently (a last interglacial non-finite-age wood, AVR-PAL-07; middle Holocene wood, FIRI-F standard) and the resulting ^{14}C values were within expected ranges (Table S2). The ^{14}C ages were calibrated using Bomb13NH1 (Hua et al., 2013) and IntCal13 (Reimer et al., 2013) calibration curves as appropriate with Oxcal v4.2 (Bronk Ramsey, 2009a).

3.3.2 ^{210}Pb, ^{137}Cs and ^{241}Am dating

The uppermost sections of the six peat cores were analysed by gamma spectrometry for the natural fallout radionuclide ^{210}Pb and artificial fallout radionuclides ^{137}Cs and ^{241}Am. The measurements were carried out using ultralow background gamma spectrometers (ORTEC, Oak Ridge, TN, USA) at the University of Alberta equipped with ORTEC GWL-250-15 HPGe well detectors (with OFHC Cu endcap and high purity Al well tube) in an ultralow background J-type cryostat surrounded by a virgin lead shield (15 cm thick) with nitrogen purge port. Full details are reported in Appendix B.

Unsupported ^{210}Pb activity was calculated by subtracting supported ^{210}Pb (assumed to be in equilibrium with ^{226}Ra activity) from the measured total ^{210}Pb activity. Since individual ^{226}Ra measurements at some sites (ANZ, UTK, McM) had very large relative uncertainties (70% on average), supported ^{210}Pb activity was in practice calculated as the running average of the nearest three ^{226}Ra values. A similar smoothing process was applied to the raw ^{241}Am data.

Raw ^{210}Pb dates were calculated using Constant Rate of Supply Model (CRS, Appleby and Oldfield, 1978). This assumes a constant rate of supply of unsupported ^{210}Pb to the peat surface despite variable sedimentation rates - an appropriate assumption for ombrotrophic peatlands where mass specific concentrations can change through time as the result of organic decay. Peaks in the ^{137}Cs and ^{241}Am records were used to identify, where possible, the 1963 depth, which relates to the maximum fallout values of these radionuclides from the atmospheric testing of nuclear weapons.

3.4 Bayesian age modelling

Age-depth models were constructed using OxCal's Poisson process model (*P_Sequence*, Bronk Ramsey, 2008). Two steps were followed for each site: first, independent models for each chronometer were visually compared for the initial detection of outliers and/or offsets between the dating methods. This is more effective as a first approach than using statistical techniques that can be biased by, for example, the high number and tight distribution of ^{210}Pb dates presented here. Cryptotephra isochrons were used as independent checks for both radiometric methods and the data were corrected where necessary. The resulting radiometric data for each site were then combined in one *P_Sequence* model and outliers were judged statistically using OxCal's agreement indices (AI), showing the extent to which the modelled posterior distributions overlap with the original distributions, and a student t-distribution outlier model (Bronk Ramsey, 2009b).

The *P_Sequence* model in OxCal v4.2 is the most appropriate for modelling peat ages as it allows variable accumulation rates. Here the k parameter - deposition events defined as increments per unit length, controlling model rigidity and resolution - was set as variable rather than fixed to increase flexibility of the model (Bronk Ramsey, 2013). Furthermore, OxCal's boundary function can constrain the models using identified changes from supporting data (detailed in *Section 3.1*). This function does not force a change or require a hiatus to occur, but instead allows a break point in accumulation rates if the model shows the dates are statistically best represented that way.

4. Results

Summaries of core data produced from all six sites are plotted in Figure 2, including stratigraphic units, event boundaries, cryptotephra shard concentration profiles, and loss on ignition percentages (LOI). Depths where cryptotephra samples were not

295 analysed are shown as dots. The individual model components (age data and event
296 boundaries) are discussed in detail before the full models are assessed. We focus on
297 the post-industrial period (post AD 1850) as all three methods have data available and
298 a more thorough comparison is therefore possible. This period also relates to peat
299 depths that will contain the acrotelm/catotelm boundary.

300 Multiple model iterations were developed for each site as new data (ages and event
301 histories) were produced– these are fully documented in Figures S2-7, and only the
302 final versions are presented here.

303 4.1 Event histories

304 Proxy data used to define events in the core histories that are included as boundaries
305 in our models are shown in Table 1, and the event depths are presented as red dashed
306 lines in Figure 2 and Figures 5-7.

307 Recorded events at these peatlands are predominantly local fires interpreted using
308 abundances of charcoal >1 mm and charred macrofossil remains (e.g. *Picea* needles,
309 *Sphagnum*, Ericaceae leaves; Magnan et al., 2018). These fires may have burned some
310 of the upper peat layers and created a hiatus in the peat sequence. After a fire, some
311 studies have shown that mechanisms of interception and retention may change - as
312 organic matter becomes more hydrophobic re-wetting is reduced and runoff increases
313 (e.g. Certini, 2005, and references therein). Shifts towards drier surface conditions, as
314 interpreted from changes in moss assemblages and the increased presence of conifers,
315 could have changed rates of peat accumulation or decomposition. Three sites (ANZ,
316 McM and UTK) have evidence for permafrost aggradation interpreted from drying of
317 the bog surface (reconstructed using testate amoebae; van Bellen et al., submitted),
318 increased degree of peat humification, changes in plant communities, and stable

isotope signature (Magnan et al., 2018). The permafrost at these sites most likely formed as ice lenses that would have caused an upheaval and drying of the peat surface, a major slowdown in peat accumulation, and the development of internal lawn after thaw (Zoltai and Tarnocai, 1975; Vitt et al., 1994).

Not all events are included in the models – particularly further back in time where multiple boundaries may occur between measured dates and including both boundaries would cause a break in the model. However, peat accumulation rates in these periods are an order of magnitude lower relative to the modern period (0.01-0.05 cm/year vs 0.25-1.55 cm/year) as the peat has been compressed and has been subjected to a longer period of decay before burial in the catotelm, and it is unlikely that boundaries relating to short-term events (e.g. fires in one season/year) would significantly impact accumulation rates.

4.2 Cryptotephra results

Glass shards are present at all sites in both intervals sampled (<~200 yr BP, and surrounding AD 853), although the shard concentration profiles vary between sites. Figure 2 shows the profiles for both intervals, with light grey bars showing 10x values as the shard counts in the two periods differ by an order of magnitude. The sites preserve different numbers of peaks within the studied intervals and have different physical taphonomic processes affecting shard preservation (e.g. maximum peak concentrations, shard dispersion below the identified peak).

Sixteen potential airfall peaks were identified for geochemical analysis. Table 2 and Figures 3 and 4 show the samples analysed, the average major element data EPMA for identified geochemical populations, and any possible geochemical correlations to known eruptions with associated chronological data that can be included in our age

343 models. Full normalised single point major element EPMA datasets are provided in
344 Table S1.

345 Nine samples can be used as isochrons as they are identified as primary airfall events
346 (where one dominant geochemical population is present) and correlate with reference
347 material for known eruptions (Novarupta-Katmai 1912, UA 1364, and the eastern
348 lobe of the White River Ash, WRAe, UA 1119; UA reference collection samples,
349 details provided in Table 2). Six of the remaining samples (McK 36, ANZ 40-44, MIL
350 57) have mixed geochemical data likely resulting from disrupted peat accumulation
351 and/or preservation (e.g. removal of organic material by fire) and one sample (UTK
352 36) has insufficient data for comparison.

353 In the late Holocene interval analysed here (up to 800 years surrounding AD 853),
354 four of the sites preserve a clear peak in glass concentration of over 8,000 shards/cm^3
355 (ANZ, UA 2919; JPH, UA 2873; McK, UA 2877; and UTK, UA 2924). A smaller
356 peak (~1500 shards/cm^3) is present in McM (UA 2920) and MIL has background
357 level counts. There are additional geochemically distinct secondary peaks present
358 stratigraphically below the primary peak at JPH and above the primary peak at McK
359 and UTK (Figure 2). These are not discussed further here as they have not been
360 correlated between the cores and do not have associated chronological information.

361 The primary peaks identified at five sites correlate geochemically with the WRAe
362 tephra (Figure 3). Glass from MIL is mixed – geochemically some shards correlate
363 with WRAe, as well as other more mafic populations. An isochron is not defined here
364 as the shard concentration profile is likely reworked given the relatively low shard
365 counts with mixed geochemistry and the increased presence of silts (20-70% mineral
366 content) in this minerotrophic section of the core.

Shard concentrations for the surface peat records are shown in more detail in Figure 5 alongside summarised age modelling data (see *Section 4.3* for details). Both ANZ and McK were analysed from the surface back to ~AD 1800 and significant concentrations of glass were absent for most of the 20th century. A primary peak of ~80-210 shards/cm^3 is seen at all sites, with samples at McK having higher concentrations of up to ~600 shards/cm^3. The shard profiles are highly variable between sites with some features only present at selected sites e.g. an older secondary peak at ANZ; significant tails of shards at JPH and McM (Figure 2).

Glass correlating to the Alaska eruption of Novarupta-Katmai in 1912 is present at four sites (ANZ, UA 2969; JPH, UA 2913; McM, UA 2920; and MIL, UA 2914; Figure 3). This is the southern-most occurrence of Novarupta-Katmai 1912 to date, and the second reported identification in North America outside of Alaska. The only previous distal correlation of Novarupta-Katmai 1912 is with glass in Greenland's North Grip ice core (Coulter et al., 2012).

The primary peak in McK (UA 2966) has at least three distinct geochemical populations that appear Aleutian in origin (although their alkali totals are relatively high) but have no identified correlations (Figure 4). As the peak shard counts are significantly higher than recorded at other sites this is interpreted as an over-concentration of glass, most likely caused by a period of reduced peat accumulation or the removal of organic material. Supporting proxy data show a shift at this depth from wet to dry conditions but no evidence of fire.

The broad peak of shards at ANZ from 38.62-42.89 cm (UA 2907, 2908, 2909, 2967, 2971) contains multiple geochemical populations - two can be correlated to Novarupta-Katmai 1912 and Mt. Churchill, and one appears correlate to ash bed Z, a mid-1600s eruption of Mt. St. Helens (Figure 4). Ash bed Z is recorded proximally in

Washington as a thin deposit of fine ash with a NE trajectory, maximum thickness of 15cm, and a similar geochemical composition to the pre-1980 summit dome (Mullineaux, 1996). Stratigraphically, it occurs between set X (~AD 1500s) and set T (~AD 1800s) and is estimated to have erupted in the mid-1600s (Yamaguchi and Hoblitt, 1995). Ash bed Z is interpreted as a co-ignimbrite ash that would be unlikely to travel as far north but there are no other known Mt. St. Helens eruptions that have the same high wt.% SiO_2 content. The most recent eruptive activity from Mount Churchill is reported at ~AD 1640-1665 (Payne et al., 2008).

4.3 Radiometric data

4.3.1 ^{14}C dates

All ^{14}C dates reported here followed their observed stratigraphic order (Table 3) although several dates were bimodal or multimodal when calibrated, especially around the 19th century. This is common for ^{14}C dates from this time period due to the shape of the calibration curves – the pre-bomb curve (IntCal13, Reimer et al., 2013) plateaus and results in very broad calibrated ages, while the bomb curve (NH1, Hua et al., 2013) has a sharp asymmetrical peak resulting in bimodal dates, with an artificial over-representation from 1956-1963 when the ^{14}C signal rapidly increased. Dominant peaks can be identified using, for example, the rising shoulder of the bomb peak, or by modelling multiple dates in stratigraphic context. At McM (#38 – 42.49 cm, #42 – 47.02 cm) and McK (#40 – 45.92 cm, #50 – 57.90 cm) large apparent jumps between dated samples occurred, indicating the presence of either hiatuses or significant changes in accumulation rate. At the three of the four sites (excluding MIL) where Novarupta-Katmai 1912 is present the cryptotephra peak agrees with the ^{14}C one sigma error range.

4.3.2 ^{210}Pb, ^{137}Cs and ^{241}Am dates

Key parameters associated with each core, including the maximum ^{210}Pb activity, the ^{210}Pb and ^{137}Cs inventories, and the mean ^{210}Pb flux, are summarised in Table 4, and full details of the radiometric data determined for each core are shown in Table S3a. Measured ^{226}Ra concentrations were an order of magnitude lower than those typical of mineral soils with mean values of around 5 Bq kg^{-1} - this is assumed to reflect the high organic matter content of the bogs. The ^{210}Pb radiometric inventories are broadly similar and correspond to mean ^{210}Pb supply rates of between 73-119 Bq m^{-2} y^{-1}, with a mean value of 97 Bq m^{-2} y^{-1}. Although there is very little data on ^{210}Pb fallout in this region, these are comparable to published values for atmospheric flux (e.g. Appleby and Oldfield, 1983; Bauer et al., 2009; Turetsky et al., 2007; Wieder et al., 2016).

Records of ^{137}Cs activity versus depth and initial ^{210}Pb dates calculated using the CRS model for all sites are shown in Figure 5. Many of the cores show evidence of significant modification of the ^{137}Cs fallout record that is expected to reflect fallout from the atmospheric testing of nuclear weapons beginning in the mid-1950s and reaching a peak in 1963. Implementation of the atmospheric test ban treaty in 1963 resulted in a rapid decline in fallout to very low levels by the mid-1980s, and fallout from the 1986 Chernobyl accident in this region was negligible. Post-depositional transport processes have resulted in significant discrepancies between the bog records and the fallout record (Figure 5), making identification of the 1963 depth problematic. Unusual features include multiple peaks and increasing concentrations towards the top of the core. Regarding the surficial peaks, the enrichment of alkali metals at the surface of bogs is known to be related to biological uptake by plants (Damman, 1978) rather than a reflection of direct atmospheric inputs. Cs-137 is recorded elsewhere as being mobile in acidic peat bog profiles (e.g. Appleby et al., 1997; MacKenzie et al., 1997; Schleich et al., 2000; Zaccone et al., 2007).

While the 1963 dates for these cores are lacking in precision, they are in reasonable agreement with the ^{210}Pb dates (Table 5) but only three cores (ANZ, McK, UTK) had ^{137}Cs records that could be used to establish the 1963 depth with some confidence.

Although the ^{137}Cs record in ANZ has two distinct peaks, at 18-21 cm and 32-37 cm, evidence that the deeper peak records 1963 is provided by its location below the 28.45 cm sample dated by ^{14}C to 1974, and the presence at around the same depth (34-37 cm) of a small but significant ^{241}Am peak. McK and UTK both have single prominent well-defined ^{137}Cs peaks, at 30 cm (McK) and 30-34 cm (UTK). 1963 dates for these features are supported by the fact that both lie just below samples dated by ^{14}C to the mid to late 1960s: the 28.58 cm in McK is dated 1965-6, and the 32.5 cm in UTK sample is dated 1969-70. In UTK there is also a small but significant ^{241}Am peak at the same depth as the ^{137}Cs peak. The raw ^{210}Pb dates for these cores are also in general agreement with the ^{137}Cs dates - at the McK core they place 1963 at a depth of 30 cm, very close to the ^{137}Cs peak. However, there is a small discrepancy for UTK as the raw ^{210}Pb calculations place 1963 at 34.75 cm, and a slightly larger discrepancy for ANZ where 1963 is placed at a depth of 31.2 cm.

In the other three cores it was only possible to give some general indication as to the 1963 depth. In JPH the ^{137}Cs record has two prominent peaks, at 1.5 cm and 6 cm, neither of which are likely to record the 1963 fallout maximum. It may however be recorded by a small but diffuse ^{241}Am peak at 11-14 cm. In McM there is a broad ^{137}Cs feature that includes two distinct peaks, at 17-19 cm and 23 cm. Small concentrations of ^{241}Am between 20-27 cm suggest that the deeper though smaller ^{137}Cs peak dates from the early 1960s. In MIL there are again two well-resolved peaks, the larger at 24 cm and the smaller at 31-34 cm. Traces of ^{241}Am were recorded between 28 and 34 cm.

For comparisons with the cryptotephra data, the raw CRS model dates for ANZ place 1912 at a depth of 37.8 cm, in good agreement with the Novarupta-Katmai tephra date for this core (1912=37.6 cm). At the other four sites with this marker, however, there are significant discrepancies between the tephra and ^{210}Pb dates (Table 5). Causes of these discrepancies, and those between ^{210}Pb and ^{137}Cs dates, include variations in the rate of supply of ^{210}Pb due to localised changes at the surface of the bog, post-depositional downwards migration of ^{210}Pb, and hiatuses in the core record. These can all result in failure of the ^{210}Pb record to fully meet the assumptions of the CRS model. Corrected ^{210}Pb dates can be obtained by instead applying the CRS model in a piecew3ise way using those clearly identifiable chronostratigraphic dates as reference points (Appleby 2001). Pb-210 dates determined by this method are given in Table S3b. ^{137}Cs and tephra dates used as reference points in the calculations are shown in bold.

4.4 Age-depth modelling and comparison of chronometers

As a manual first pass to compare the radiometric methods, dates produced from ^{14}C and ^{210}Pb were modelled in separate *P_Sequence* models and compared with each other and the independent chronostratigraphic markers (^{137}Cs, ^{241}Am, and cryptotephra). Figure 5 shows the mean modelled ^{14}C and ^{210}Pb values for each sample plotted with 1 sigma error ranges. At UTK the initial ^{210}Pb, ^{14}C, and ^{137}Cs data agree well - most offsets are less than 5 years. The upper section of MIL is similarly agreeable. At the remaining four sites, ^{210}Pb dates are commonly offset from ^{14}C dates by ~10 years back until 1960, and consistently underestimate the modelled ^{14}C ages by 20 to more than 100 years from 1960-1850.

Figure 6 shows that the recalculated CRS ages (^{210}Pb corrected, where possible, using cryptotephra and ^{137}Cs) for MIL and McM are in better agreement with the ^{14}C ages,

492 while JPH has agreement between the ^{210}Pb dates, ^{137}Cs, and tephra record but the ^{14}C
493 dates are offset. ^{210}Pb data from ANZ were not corrected as the offset in the lowest
494 three dates from 36-40 cm appears to be directly related to the presence of permafrost.
495 Instead, a calendar date for the 1912 eruption was included in the model.

496 The resulting *P_Sequence* models for five of the six sites (Figure 7) have improved
497 agreement indices (AI), more realistic accumulation rates, and improved precision
498 when compared with any one chronometer alone. For the 20th century, the combined
499 models for four sites (ANZ, JPH, McK, McM) have standard deviations of less than 5
500 years for all samples. MIL and UTK have one and five samples respectively that have
501 standard deviations of up to 7 years. UTK has a number of increased errors at the start
502 of 20th century due to the presence of permafrost directly above two radiocarbon-
503 plateau dates which cannot be more tightly constrained with the current prior dataset.

504 The models are classified here as simple (MIL, UTK), advanced (McM, ANZ), and
505 complex (JPH, McK). Simple models are well constrained and have good agreement
506 between the chronometers with little to no additional work needed. Advanced models
507 have some complications, e.g. prolonged disruptions to accumulation by the presence
508 of permafrost or local surface peat combustion, but the corrected data agree well when
509 this additional information is included in the model. Complex models have
510 disagreements between chronometers which cannot be fully resolved with the current
511 data sets or cannot be fully explained.

512 Using outlier analysis as a second pass after manual removal of outliers, 1-3 dates
513 from the period back to ~AD 1850 are rejected at each site (excluding UTK which
514 includes all dates), as well as one date from the older section at McM and MIL. At
515 MIL three dates from 32-36 cm are identified as outliers (one ^{14}C, two ^{210}Pb; Figure
516 5); this period is also associated with changes in dry density, C/N and ligneous roots.

For JPH a successful model only includes the tephra-corrected ^{210}Pb data and excludes all three modern ^{14}C dates.

5. Discussion

The data shown here demonstrate the range of variability that can occur when constructing age-depth models for peatland records, even within one region. None of the chronological methods are intrinsically problematic, but they rely on assumptions of relatively uniform peat accumulation and signal preservation that may be invalid for parts of records or changes over time. While some sites can be modelled simply, at most sites a more detailed comparison using multiple chronometers and environmental proxies that affect peat accumulation and preservation is useful to assess accuracy. Dating modern peat cores with a single chronometer can mask this complexity, particularly in peatlands affected by strong environmental changes (e.g. permafrost formation or surface drying that may affect accumulation rates) with the caveat that inaccuracies in age models can lead to incorrect interpretations of associated proxy data.

5.1 Environmental histories

Environmental histories record events which may have impacted the peatland archives, but here they have not all noticeably affected the peat surface and resulting modelled accumulation rates. For example, possible fires recorded at MIL and UTK do not appear to have combusted peat surface material at the coring locations, although an older local fire at MIL at 44 cm coincides with a sharp change in accumulation rate. At five sites, there is an ecological shift towards a dominance of *Sphagnum* section *Acutifolia* during the 20th century. These changes are not coincident, with JPH starting in ~1956, MIL in ~1965, and ANZ, McM and UTK, all

541 in 1980-1985, but this change only appears to affect accumulation rates at two of the
542 preserved records (McM and UTK).

543 Three sites have apparent hiatuses through either loss of organic material or
544 significant reductions in accumulation. At ANZ, ~200 years of peat is missing from
545 ca. AD 1700-1900 during a period of permafrost and local fires as shown by the
546 bracketing ^{14}C and tephra data. Bracketing ^{14}C dates at McM show an apparent hiatus
547 during the period of permafrost and local fires which coincides with the Little Ice Age
548 (47.02 cm = ~AD 1100, 42.29 cm = ~AD 1700). At McK, a level corresponding to a
549 wet to dry shift in the late 19th century (42 cm) has a concentration of glass from at
550 least three different eruptions, interpreted here as evidence for a near stationary
551 peatland surface that accumulated multiple tephra falls. These 'hiatuses' occur over
552 discrete depths of the peat records, and can only be properly accounted for when
553 recognised using multiple techniques.

554 Permafrost, surface drying, local fires, and ligneous roots are the features most
555 commonly associated with complications in the resulting age-depth models. Possible
556 permafrost development was identified at three sites, although the timing is not fully
557 coincident. Both McM and ANZ record an early onset (AD 1300 & 1600) while UTK
558 has 20th century onset (~AD 1900). McM shows the earliest disappearance at ~AD
559 1850, while at ANZ and UTK permafrost has persisted until 1960-1970.

560 The inclusion of environmental histories that may have affected peat accumulation
561 rates as boundaries in OxCal *P_Sequence* models is appropriate to judge the relative
562 importance of events identified from proxy data as the dates can confirm if events had
563 coincident changes in peat accumulation rates. The models produced here show that
564 this information is important for obtaining an accurate representation of peat
565 accumulation, particularly where hiatuses and significant peat accumulation changes

have occurred. Using environmental information to produce a Bayesian model of ^{210}Pb data calculated using the CRS model also combines the two methods in a way that provides better agreement with other complimentary data and results in dates based on physical principles.

The precise age of these boundaries must be considered cautiously, however –if intervals do not have *a priori* constraining dates close to the depths of the boundary change they will have relatively broad associated errors and ranges of possible accumulation rates above and below. Several dates here were sampled at the exact depth of the boundary and it is not necessarily clear if they represent maximum or minimum constraints e.g. for local fires the material may be the subsequent new peat growth or the lowest depth burned down to. This can be addressed by dating directly below the event/boundary to obtain a maximum age if the event is of particular interest.

5.2 Cryptotephra data

Tephra data from these sites extend the known geographical limits for deposition of Novarupta-Katmai 1912 and the regionally widespread WRAe. While our tephra profiles are not fully comprehensive late Holocene records for the area, they demonstrate the preservation of tephra that are both locally important and widespread, and hence the possibilities for correlation with other regional to hemispheric records.

The identification of 17th century tephra including a Mt. Churchill correlative and the MSH ash bed Z shows the potential for other cryptotephra horizons in the region. Both tephra were erupted within the bracketing ^{14}C dates at ANZ (Table 3). Only 2 cm of peat is present between tephra peaks from 1912 and the mid 17th century beds and this is coincident with the presence of increased charcoal and charred

590 macrofossils. We interpret this as burning of surface peat at ANZ before AD 1900
591 that removed peat accumulated since ~AD 1700 and concentrated glass preserved
592 from this period.

593 The shard profiles reported here support previous work reporting spatial variability of
594 the number of tephra and shard concentrations preserved regionally (e.g. Watson et
595 al., 2015; Zoltai, 1989): Novarupta-Katmai 1912 was seemingly absent from McK;
596 WRAe was not identified at MIL, though this is not surprising given that the peatland
597 was a fen at the time and not ombrotrophic.

598 5.3 Age-depth models

599 Age-depth models incorporate information from multiple analyses and additional
600 supporting methodologies, and can highlight periods of disagreement between dating
601 methods that have their own inherent strengths and weaknesses. This study does not
602 seek to give primacy of one dating technique over another — a positive outcome here
603 is that modelling a range of independent techniques allows the slight biases that exist
604 within a method to be interrogated and considered within the light of the total
605 chronological information available, ultimately providing more robust chronologies.

606 C-14 dates are commonly used for peatland age models, but often only pre-bomb
607 dates will be connected to the bottom of a ^{210}Pb record. Three sites here show good
608 agreement between post-bomb ^{14}C dates and ^{210}Pb, with both methods producing
609 well-constrained age models back through the 1960s. However, at JPH three post-
610 bomb dates were shown to be outliers and statistically rejected from the Bayesian
611 models. As macrofossils were carefully picked and identified it is unlikely that these
612 outliers were the result of, for example, root contamination. Instead, very low rates of
613 peat accumulation for the upper layers likely means each dated sample is comprised

614 of material from multiple years of accumulation (Garnett and Stevenson, 2004) and
615 the resolution of ^{14}C analysis is not comparable to the ^{210}Pb dates.

616 It is generally accepted that ^{210}Pb dating in peatlands needs independent corroboration
617 (Oldfield et al., 1995) and there was reasonable agreement between the raw CRS
618 model ^{210}Pb dates and the ^{137}Cs dates where they could be discerned. In this study, we
619 analysed cores primarily for the reconstruction of atmospheric deposition of
620 contaminants in the Athabasca Bituminous Sands region since commercial
621 development in AD 1967. The time frame of importance for these studies, focused on
622 the post-bomb interval, is well constrained within these cores and the age differences
623 between the methods are relatively small.

624 Offsets between ^{14}C and ^{210}Pb are more common for the pre-bomb interval through
625 the 20th century where both methods have increased uncertainties, but ^{14}C dates
626 helped highlight large hiatuses from reduced peat accumulation or lost organic
627 material that were not clearly shown in the ^{210}Pb profiles. Discrepancies between the
628 raw ^{210}Pb dates and the chronostratigraphic dates were largely resolved by applying
629 the CRS model in a piecewise way using the methods outlined in Appleby (2001).

630 Pre-bomb ^{210}Pb dates are consistently younger than ^{14}C dates from the same levels.
631 This is unlike some previously reported discrepancies between ^{210}Pb and ^{14}C dates
632 from European peats (e.g. Fiałkiewicz-Kozieł et al., 2015; Goodsite et al., 2001; Van
633 der Plicht et al., 2013), and instead the trend is similar to that reported from Sweden
634 (Oldfield et al., 1997), Poland (Piotrowska et al., 2010), and Saskatchewan (Bauer et
635 al., 2009). Uncertainty in raw ^{210}Pb dates calculated using either of the standard
636 simple models are less securely known as the records extend beyond the ^{137}Cs peak to
637 ~100 years. By the early 20th century ^{210}Pb concentrations have decayed to just 4% of
638 their original value. Discrepancies in the older parts of the records here where there is

639 recorded ^{210}Pb activity below its excepted depth of equilibrium are most probably due
640 to some downwards migration of ^{210}Pb within the sequence. Possible causes include
641 chemical and physical diffusion, and may relate to the development of permafrost and
642 movement of water within the peatland (see *section 5.4* for full discussion).

643 Cryptotephra primary air-fall peaks and overlapping ^{14}C dates provide additional data
644 for the age models by highlighting periods of complexity (e.g. permafrost, hiatuses).
645 This represents a novel use of historic cryptotephra — i.e. having a reliable early 20th
646 century chronostratigraphic date to identify and correct errors in the ^{210}Pb dates for
647 that part of the record. This tephra is particularly well timed for such a comparison as
648 it occurs just after the plateau in the radiocarbon calibration curve that causes
649 increased errors in ^{14}C dates from ~AD 1700-1900 and over just 4 half-lives of ^{210}Pb
650 before the present day, when the signal uncertainty is increased. Furthermore,
651 interruptions to peat accumulation are reported here at several sites in Alberta at this
652 time; these events can be constrained more thoroughly when associated with tephra
653 air-fall peaks.

654 5.4 Chronological signal preservation and limits to age-depth model resolution

655 The measured signal for each chronological technique has different physical
656 properties and therefore differing potential for offset from the true age of the record.
657 For example, our results show that post-depositional migration had a much greater
658 impact on the ^{137}Cs records than ^{210}Pb or cryptotephra shards. While this is expected
659 given previous studies on the mobility of ^{137}Cs within ombrotrophic bogs (e.g.
660 Appleby et al., 1997; Schell et al., 1989; Schleich et al., 2000; Zaccone et al., 2007)
661 variation in chronological signal stability and preservation for the methods used (^{14}C,
662 ^{210}Pb, ^{137}Cs, ^{241}Am, cryptotephra) is discussed here. A variety of processes affecting
663 signal variation and the physical characteristics of the peat substrate must be

664 considered as well as the chronological signal. Together, these factors relate directly
665 to the realistic limit of the accuracy of age-depth models and the temporal resolution
666 of proxy records from peat archives. This is assessed here using four key questions –
667 What is the measured signal? How is this signal fixed in peat deposits? How can this
668 signal change or be mobilised? And what external characteristics are important for
669 accurate signal preservation?

670 There is a large body of literature addressing each aspect considered here— we
671 summarise central themes and focus on the most relevant points for the data presented
672 here. Analytical uncertainty associated with the processing and measurement of
673 sample signals are not discussed here as they are assumed to have been accounted for
674 in the error propagation for individual dates, the initial evaluation and inter-
675 comparison of the datasets, and the statistical age-depth modelling process. We also
676 do not directly address whether there is an offset between the age-depth relationship
677 for the peat and the age-depth relationship for the associated environmental proxies.
678 Given the observable differences in factors affecting preservation this may occur,
679 although to what degree needs further investigation.

680 5.4.1 What is the measured signal and how is this fixed in peats

681 For signal source, ^{14}C values result from the fixing of atmospheric CO_2 during
682 photosynthesis while the other methods rely on atmospheric fallout and retention of
683 inorganic particles. C-14 signals are set when the living material dies as the organism
684 is no longer in equilibrium with the atmosphere. Anomalous results can result from
685 the sample having a misleading signal due to uptake of old or modern carbon sources
686 - ^{14}C values can be dampened by uptake of old-carbon from older plant material
687 within the sequence (e.g. Goslar et al., 2005; Kilian et al., 1995) or industrial pollution
688 (e.g. Chambers et al., 1979; Charman and Garnett, 2005).

For the inorganic particles, a stratigraphic signal is preserved by the chemical or physical retention of the particles by the peat matrix after direct air-fall on to the bog surface. Variations in the relative concentration of the signal imply changes in the surface retention over time, assumed to relate to changing atmospheric concentrations and peat accumulation rates. However, there can be variations in the initial infiltration depth of the particles at the surface (e.g. Dörr, 1995; Olid et al., 2016), the effective preservation rate of the atmospheric signal (e.g. particle interception, the physical entrapment of particles by the peat matrix, location specific factors), and surficial reworking before the signal is fixed (e.g. microtopography, snow cover). Once associated with the peat surface, signal retention can be linked broadly to chemical (e.g. adsorption and complexation of particles and ions to peat surfaces, affected by redox potential, pH and organic acids in pore waters), biological (e.g. root uptake, plant growth), and hydrological controls (e.g. infiltration with precipitation, water table change, permafrost, downwashing, evapotranspiration).

5.4.2 How can this signal change or be mobilised?

As mosses do not have roots and absorb water and nutrients mainly through their leaves instead of the substrate, moss ^{14}C dates are most likely affected by material being preserved at a different stratigraphic position from the contemporary surface due to mechanical processes (e.g. reburial or re-deposition of organic material, penetration of living rootlets in to older layers), or the assimilation of material from multiple years in one analysed sample (Garnett and Stevenson, 2004; Piotrowska et al., 2010). Organic material from other (non-bryophyte) plants and organisms present in a peatland may be more commonly affected by the uptake of either old or modern carbon sources as mentioned in 5.4.1. As ^{14}C dates are independent of each other, it is possible that changes in peat accumulation may not be fully constrained by the

714 number of dates produced if they occurred between dated intervals, or within only a
715 few cm of accumulation.

716 The inorganic particles used here differ in size by orders of magnitude (Figure 8a) –
717 ^{210}Pb, ^{137}Cs, and ^{241}Am are attached to sub-micron aerosols (~0.5 μm in diameter)
718 while cryptotephra shards are typically 10-100 μm. These differences will affect
719 particle interception by the bog surface (differential deposition) as well as the
720 retention of these two types of particles (diagenetic modification).

721 For metal ions in mineral soils, relative mobility is a function of both the physical and
722 chemical characteristics of the metals themselves (mainly ionic radius and electrical
723 charge), as well as soil features, including pH and redox potential, and abundance of
724 clay minerals, oxyhydroxides, and organic matter content (Degryse et al., 2009). Lead
725 ions, for example, form stable complexes with organic matter, oxyhydroxides, and
726 clay minerals which act in concert to reduce the mobility of Pb^{2+} (Ferraz and
727 Lourençlo, 2000; Strawn and Sparks, 2000; Trivedi et al., 2003; Syrovetnik et al.,
728 2007). However, while free ions in solution are typically the most reactive species,
729 ^{210}Pb and other forms of atmospheric Pb are not predominantly in ionic form and
730 other mechanisms are required to understand metal retention at the air-bog interface,
731 starting with mosses (Shotyk et al., 2015). Variations in pH can profoundly affect Pb
732 adsorption (Grybos et al., 2007) and it has been suggested that ^{210}Pb may undergo
733 some detachment from its host aerosol in response to the low pH of bog surface water
734 (approximately pH 4) or acidic rainwater (Shotyk et al., 2015).

735 Several studies have examined the potential mobility of stable and radioactive Pb
736 isotopes in peat sequences in recent decades after reported findings of profiles or flux
737 values that do not correlate with independent markers, or differences between features
738 such as hummocks and hollows within one peatland (Damman, 1978; Oldfield et al.,

739 1979; Urban et al., 1990; Lamborg et al., 2002; Hansson et al., 2014). For some peat
740 profiles in Alberta it has been reported that ^{210}Pb concentrations did not decrease
741 exponentially with depth or approach a low constant value (Turetsky et al., 2000;
742 Wieder et al., 2016) and ^{210}Pb dating is therefore not possible due to insufficient
743 signal preservation. Multiple studies internationally, however, have produced
744 measured profiles and comparisons with established pollen-stratigraphies, pollutant
745 histories, independent chronological techniques, herbarium samples and records from
746 other sites, leading to the conclusion that there was no measurable post-depositional
747 migration (Jones and Hao, 1993; Shotyk, 1996; Appleby et al., 1997; Vile et al., 1999;
748 Weiss et al., 1999; de Vleeschouwer et al., 2009; Novák et al., 2011; Pratte et al.,
749 2013; Shotyk et al., 2016b).

750 For the other radioisotopes analysed here, ^{241}Am is considered to be relatively stable
751 and in good agreement with other chronometers (Oldfield et al., 1995; Smith et al.,
752 1997; Testa et al., 1999; Schleich et al., 2000; Gallagher et al., 2001; Łokas et al.,
753 2013). Cs-137 records are more variable. Some studies show expected peaks and good
754 agreement with established chronometers, but the isotope can be highly mobile in
755 acidic bog-water or decomposing organic material, although a small percentage of
756 mineral matter may improve its retention (Schell et al., 1989; MacKenzie et al., 1997;
757 Sokolik et al., 2002; Zaccone et al., 2007; Lusa et al., 2015). Even with some degree
758 of post-depositional migration, these fallout radionuclides can still be used to evaluate
759 other chronometers if there is a peak in the profile corresponding to the zenith of
760 atmospheric fallout. Multiple peaks or a blurred signal, however, are not easy to
761 utilise.

762 The majority of cryptotephra shards have been shown to remain at the surface where
763 they were deposited - there is evidence for some migration laterally within a peatland,

764 and vertically in a peat sequence, but this does not tend to obscure the primary
765 depositional horizon (Payne et al., 2005; Payne and Gehrels, 2010; Watson et al.,
766 2015). Vertical displacement is most likely to occur soon after deposition unless it is
767 caused by external disturbances (e.g. fires; Payne and Gehrels, 2010). While there is
768 no discussion of the mechanism by which shards are fixed to peat deposits in the
769 literature, it is assumed this is a physical rather than chemical process. Movement
770 within the peat stratigraphy can be observed as tails above or below a primary shard
771 concentration peak or mixed geochemical signals where different populations are
772 combined, while lateral movement results in variable peak concentrations between
773 cores. These effects, however, can both also be caused by secondary deposition if
774 tephra shards are reworked on the landscape, or from multiple eruptions that are
775 closely spaced in time. This is unlikely to be significant within an ombrotrophic
776 peatland, although deforestation and increased wind erosion in the surrounding area
777 could be a significant external influence.

778 5.4.3 What external characteristics are important for accurate signal preservation?

779 Locally important processes of redistribution for any particles within a peatland
780 include (Figure 8b): i) variable microtopography allowing particles to be blown or
781 washed from exposed areas to hollows ; ii) direct airfall on to snow, with
782 redistribution by surface winds, and secondary deposition from the temporary surface
783 position after melt (e.g. Bergman et al., 2004); iii) disturbance events (e.g. fires,
784 human impacts) mobilising or removing particles; iv) vegetation interception, roots
785 facilitating downward migration, or plant growth causing upwards or lateral migration
786 of attached particles; and v) changes in the water table and percolation/downwash
787 causing vertical movement, including complications from vi) permafrost formation or
788 vii) permafrost thaw.

These processes can be considered for both the chronometer particles, and any organic matter or complexes they are bound to — the host material can also be redistributed mechanically by erosion and transport processes (e.g. mixing, bioturbation, infiltration, and decomposition) once the chronological signal has been retained. For example, ^{210}Pb demonstrates limited root absorption and uptake by plants, but has a strong affinity with the surface of soil particles and reports have shown a strong fixing to transported soil and sediment (van Hoof and Andren, 1989; He and Walling, 1996; Martínez and McBride, 1999; Novák et al., 2011). Peat itself is a highly complex porous substrate and particle movement within a peat sequence will relate to characteristics of the peat itself, including but not limited to: porosity, tortuosity, and hydraulic conductivity, related in turn to the bulk density and degree of decomposition, humification, and compaction. It is expected that these properties change over time with environmental and ecological variation, and 'anomalous' records may therefore reflect changes in processes unrelated to mobility of the signal particles. The presence of intact or degrading permafrost has been shown to affect trends in carbon accumulation and the nutrient status, organic matter accumulation, and chemistry of near surface peat (Turetsky et al., 2000; Robinson et al., 2003; Treat et al., 2016) which will also likely affect both particle retention and the ^{14}C signal.

At the sites shown here, the processes shown in Figure 8b may affect the peat deposits. However, the piecewise multi-chronometer approach is most appropriate to use when they are not occurring consistently and their influence on peat accumulation and/or signal preservation is variable or unknown. Here, local surface fires and hydrological changes in response to climatic variability, including depth of the water table and development/thaw of permafrost, are argued to be the most important processes affecting the peat deposits and their retained chronological signal. Leaching

or downwash is possible with the movement and flow of water (Hansson et al., 2015). In the catotelm, the metabolism of organisms results in anaerobic conditions and many elements form organometallic complexes with organic matter. However, if the water table is lowered and oxidation takes place (through percolating surface waters or exposure to air) these complexes are disintegrated, and the previously fixed elements can be transported out of the system (Franzén, 2006). Work using pollen and spores (Clymo and Mackay, 1987) has also demonstrated their potential mobility, although for cryptotephra the higher density and angular morphology of shards means the process would likely be less effective for glass (Payne and Gehrels, 2010).

The study sites are located in areas with sporadic permafrost identified between 150-700 years BP (Zoltai, 1995) and evidence for permafrost formation and thaw are seen in macrofossil records at ANZ, McM, and UTK. There are no extensive studies of the mobility of similar-sized particles within permafrost peatlands although there is discussion of deposition and particle retention in Arctic areas (e.g. Bergman et al., 2004; Łokas et al., 2013). While it might be expected that post-depositional mobility in peats is diminished under cold environmental conditions due to the reduced decomposition of organic matter, and limited bioturbation, we argue here that the changes associated with periods of permafrost development and thaw can affect signal preservation negatively. Sites within the zone of continuous permafrost in western Canada have well-preserved tephrostratigraphies (e.g. Davies and Froese, 2015), but it has not been confirmed if the same is true for sites with either discontinuous syngenetic permafrost, formed with peat accumulation, or ephemeral epigenetic permafrost, formed after peat has been deposited (Zoltai, 1993).

The formation of either type of permafrost has implications for particle mobility. The process of freezing will concentrate ions in aqueous solution by excluding them from

839 the ice, and as syngenetic permafrost commonly freezes more rapidly from the top
840 down, this process will potentially relocate any metal ions and low molecular weight
841 humic substances as dissolved organic matter to deeper layers in the peat profile.
842 Within an individual peatland permafrost formation and thaw do not affect all areas
843 equally in time or space and the occurrence of surficial ponding, new growth of
844 diverse plant communities (e.g. sedges), and other confounding factors will affect peat
845 accumulation and signal retention/mobilisation.

846 The six sites studied here show a range of environmental histories with varying
847 impacts on their chronological records. We see this clearly with disturbance events —
848 for example, the loss of organic material from burning by local fires at ANZ and
849 McM, which have left hiatuses in the records, while other fire events at many of the
850 sites have no such loss. Permafrost development and thaw, and percolation of
851 chronometer particles (or particles hosting them) likely affected records at several
852 sites, but UTK appears unaffected. All of the chronometers applied to the peat records
853 presented here have identified complexities in their preservation, but this does not
854 render them unusable — using multiple chronometers and having detailed
855 environmental histories allows identification and incorporation of these variables on a
856 site by site basis to provide robust chronological models.

857 ## 6. Conclusions

858 This study compared multiple chronometers for the modern (post AD 1800) period at
859 six peatlands in central and northern Alberta to evaluate variability in both the dating
860 methods and individual site records. The resulting datasets are combined in robust,
861 high-resolution Bayesian age models to allow accurate and precise chronologies and
862 thorough subsequent interpretations of associated proxy data (e.g. trace metals,
863 organic contaminants). While subtle differences in the chronometers occurred at five

of the six sites, the use of multiple chronometers and supporting environmental histories allowed an informed assessment of the data that resulted in well constrained models.

These models varied in their complexity, but the largest differences in chronometers were in the pre-bomb period, coincident with the development of permafrost, drying of the peat surface and local fires. Hiatuses and significant changes in accumulation rates are common in these records, and may not be detected using only one dating technique. ^{210}Pb commonly underestimates the age of sediments in this area between AD 1875-1950, most likely due to changes in peat accumulation rates, particularly where permafrost has developed. Cryptotephra isochrons have the potential to help identify chronometer offsets where they occur, and here also helped narrow the broad error ranges associated with calibrated radiocarbon dates at and before the turn of the 20th century. New reports of glass from Novarupta-Katmai 1912, Mt. St. Helens ash bed Z and Mt. Churchill also demonstrate the potential for new additions to Alberta's regional tephrostratigraphy.

At most sites there is good agreement between dating methods for the post-bomb interval, but chronological signals from the decades to centuries before this are more challenging to reconcile. There is no recommended 'one size fits all' approach for constructing these age-depth models and, as stated by previous studies, specific local environmental histories can significantly impact records at the site scale. We argue here that for sites without 'uniform' peat accumulation, where there is significant variability over time in the processes affecting both peat accumulation rates and chronological signal retention, a piecewise approach combining multiple chronological techniques, environmental data and Bayesian modelling will produce the most reliable results.

Acknowledgements

Thanks to the Natural Science and Engineering Research Council (NSERC), the Canada Research Chairs program, and Alberta Innovates (AI) for funding (special thanks to John Zhou, Brett Purdy, and Dallas Johnson). Thanks also to the University of Alberta, the Faculty of Agricultural, Life and Environmental Sciences, and Alberta Environment and Parks for munificent start-up support for the SWAMP lab. Thanks to the Canada Foundation for Innovation for a generous equipment grant and matching funds from Alberta Enterprise and Advanced Education. Thanks to Michelle Garneau (UQAM) who provided access to laboratory facilities. Thanks also to the Land Reclamation International Graduate School of the University of Alberta and NSERC CREATE for financial and logistical support of GMB, Tracy Gartner and Karen Lund for administrative support, and Pedro Henrique Simões and Cara Albright for their help in the field.

Artwork and Table Captions

Figures

1. Map showing peatland coring locations discussed in the text. Inset shows detailed locations in the Fort McMurray area. Reproduced from van Bellen et al. (submitted)

2. Stratigraphic details of six peat cores, including sedimentology, glass shard concentration profiles, boundaries, ^{14}C sample depths and LOI data. Dark grey bars for shard concentrations are raw data (shards/cm^3), light grey bars are 10x magnification. Black outline for McM shows 25x magnification for further clarification. Black dots represent samples that were not processed for cryptotephra analyses.

3. Major-element glass geochemical plots showing the correlation between material from the northern Alberta peat cores and proximal reference material from Novarupta-Katmai 1912 and WRAe. Full details of the proximal reference material are provided in Table 2.

4. Major element glass geochemical plots showing the multiple populations present in samples from ANZ and McK, compared with outlines representing analyses of reference material from Novarupta-Katmai 1912 (solid black), Mt. Churchill (WRAe; dashed blue), and Mt. St. Helens ash bed Z (dashed red). Full details of the proximal reference material are provided in Table 2.

5. Individual core age models for the modern period, showing a) ^{14}C, ^{210}Pb and cryptotephra dates; b) delta values between the median chronometer values at each depth and the associated error; c) ^{137}Cs and ^{241}Am profiles; d) tephra shard concentration profiles.

6. Individual core age models with tephra-corrected ^{210}Pb data for AD 1650-2015 at JPH, MIL, and McM. a) ^{14}C, ^{210}Pb and cryptotephra dates; b) delta values between the median chronometer values at each depth and the associated error; c) ^{137}Cs and ^{241}Am profiles; d) tephra shard concentration profiles.

7. Final Bayesian *P_Sequence* core age models. Blue areas show 1 sigma error ranges; grey lines bound 2 sigma error ranges. Median values are shown with the dashed line.

8. a) Relative size comparison of the peat macrosfossil material, cryptotephra shards, and aerosols associated with ^{210}Pb and radioisotopes considered here.

   b) Diagrams showing mechanisms for particle and surface movement in peatlands.

   i. Variable microtopography; ii. Snow cover interception; iii. Local surface fire with removal of material; iv. Vegetation interception, root penetration; v. Water table movement; vi. Permafrost formation with raised surface, frozen substrate, and exclusion of aqueous ions; vii. Seasonal thaw of the active layer.

Tables

1. Event histories for the cores analysed from each site, including the depth of the inferred changes and the proxy data used to support this.

2. Average major element geochemical data for identifiable populations of analysed tephra samples and suggested correlations. (#) = standard deviation; FeOt = total iron oxide as FeO; H2Od = water by difference.

3. Summary of 14C dates produced from the six peat cores. BC dates are shown in blue italics; starred (*) dates are interpreted as anomolous. 14C dates were calibrated using Bomb13NH1 (Hua et al., 2013) and IntCal13 (Reimer et al., 2013) calibration curves as appropriate in Oxcal v4.2 (Bronk Ramsey, 2009a).

4. Key radiometric parameters associated with each core including the maximum ^{210}Pb activity, the ^{210}Pb and ^{137}Cs inventories, and the mean ^{210}Pb flux.

5. Comparison of reference dates for AD 1963 (137Cs) and 1912 (cryptotephra) in each core with 210Pb CRS model data. *see also: Table S3b. †No isochron defined.

SI

- F.S1 – Flow diagram for age-modelling procedure
- F.S2-7 - Evolution of age-depth models. a) Raw dates, with no event boundaries or adjustments; b) Raw dates with event boundaries; c) Final models with outliers removed and tephra dates and corrected 210Pb included where relevant.
- T.S1– Major element glass geochemical data.
- T.S2 – ^{14}C standard data.
- T.S3 – Radiometric data for each core including the total and unsupported ^{210}Pb, ^{226}Ra, ^{137}Cs and ^{241}Am concentrations versus depth.
- T.S4 – Final age model output.

965 References

966 Alaska Volcano Observatory, n.d. Alaska Volcano Observatory Online Library
967 [WWW Document]. URL www.avo.alaska.edu/downloads/. (accessed 6.30.17).

968 Ali, A.A., Ghaleb, B., Garneau, M., Asnong, H., Loisel, J., 2008. Recent peat
969 accumulation rates in minerotrophic peatlands of the Bay James region, Eastern
970 Canada, inferred by 210Pb and 137Cs radiometric techniques. Appl. Radiat. Isot.
971 66, 1350–1358. https://doi.org/10.1016/j.apradiso.2008.02.091

972 Appleby, P.G., 2001. Chronostratigraphic Techniques in Recent Sediments, in: Last,
973 W.M., Smol, J.P. (Eds.), Tracking Environmental Change Using Lake
974 Sediments. Kluwer Academic Publishers, Dordrecht, pp. 171–203.
975 https://doi.org/10.1007/0-306-47669-X_9

976 Appleby, P.G., Nolan, P.J., Oldfield, F., Richardson, N., Higgitt, S.R., 1988. 210Pb
977 dating of lake sediments and ombrotrophic peats by gamma essay. Sci. Total
978 Environ. 69, 157–177. https://doi.org/10.1016/0048-9697(88)90341-5

979 Appleby, P.G., Oldfield, F., 1983. The assessment of 210Pb data from sites with
980 varying sediment accumulation rates. Hydrobiologia 103, 29–35.
981 https://doi.org/10.1007/BF00028424

982 Appleby, P.G., Oldfield, F., 1978. The calculation of lead-210 dates assuming a
983 constant rate of supply of unsupported 210Pb to the sediment. Catena 5, 1–8.
984 https://doi.org/10.1016/S0341-8162(78)80002-2

985 Appleby, P.G., Shotyk, W., Fankhauser, A., 1997. Lead-210 age dating of three peat
986 cores in the Jura Mountains, Switzerland. Water. Air. Soil Pollut. 100, 223–231.
987 https://doi.org/10.1023/A:1018380922280

988 Baird, A.J., Belyea, L.R., Morris, P.J., 2009. Upscaling of peatland-atmosphere fluxes
989 of methane: Small-scale heterogeneity in process rates and the pitfalls of
990 "bucket-and-slab" models, in: Eichelberger, J.C., Gordeev, E., Izbekov, P.,
991 Kasahara, M., Lees, J. (Eds.), Carbon Cycling in Northern Peatlands. American
992 Geophysical Union, Washington DC, pp. 37–53.
993 https://doi.org/10.1029/2008GM000826

994 Bao, K.S., Shen, J., Zhang, Y., Wang, J., Wang, G.P., 2014. A 200-year record of
995 polycyclic aromatic hydrocarbons contamination in an ombrotrophic peatland in
996 Great Hinggan Mountain, northeast China. J. Mt. Sci. 11, 1085–1096.
997 https://doi.org/10.1007/s11629-014-3167-1

998 Barber, K.E., 1993. Peatlands as scientific archives of past biodiversity. Biodivers.
999 Conserv. 2, 474–489. https://doi.org/10.1007/BF00056743

1000 Barber, K.E., Charman, D.J., 2014. Holocene palaeoclimate records from peatlands,
1001 in: Global Change in the Holocene. Routledge, pp. 210–226.

1002 Barber, K.E., Dumayne-Peaty, L., Hughes, P.D.M., Mauquoy, D., Scaife, R., 1998.
1003 Replicability and variability of the recent macrofossil and proxy-climate record
1004 from raised bogs: Field stratigraphy and macrofossil data from Bolton Fell Moss
1005 and Walton Moss, Cumbria, England. J. Quat. Sci. 13, 515–528.
1006 https://doi.org/10.1002/(SICI)1099-1417(1998110)13:6<515::AID-
1007 JQS393>3.0.CO;2-S

1008 Bauer, I.E., Bhatti, J.S., Swanston, C., Wieder, R.K., Preston, C.M., 2009. Organic

matter accumulation and community change at the peatland-upland interface: Inferences from 14C and 210Pb dated profiles. Ecosystems 12, 636–653. https://doi.org/10.1007/s10021-009-9248-2

Beierle, B., Bond, J., 2002. Density-induced settling of tephra through organic lake sediments. J. Paleolimnol. 28, 433–440. https://doi.org/10.1023/A:1021675501346

Beilman, D.W., Vitt, D.H., Halsey, L.A., 2001. Localized Permafrost Peatlands in Western Canada: Definition, Distributions, and Degradation. Arctic, Antarct. Alp. Res. 33, 70–77. https://doi.org/10.2307/1552279

Belyea, L.R., Clymo, R.S., 2001. Feedback control of the rate of peat formation. Proc. R. Soc. B Biol. Sci. 268, 1315–1321. https://doi.org/10.1098/rspb.2001.1665

Belyea, L.R., Warner, B.G., 1994. Dating of the near- surface layer of a peatland in northwestern Ontario, Canada. Boreas 23, 259–269. https://doi.org/10.1111/j.1502-3885.1994.tb00948.x

Bergman, J., Wastegård, S., Hammarlund, D., Wohlfarth, B., Roberts, S.J., 2004. Holocene tephra horizons at Klocka Bog, west-central Sweden: Aspects of reproducibility in subarctic peat deposits. J. Quat. Sci. 19, 241–249. https://doi.org/10.1002/jqs.833

Berset, J.D., Kuehne, P., Shotyk, W., 2001. Concentrations and distribution of some polychlorinated biphenyls (PCBs) and polycyclic aromatic hydrocarbons (PAHs) in an ombrotrophic peat bog profile of Switzerland. Sci. Total Environ. 267, 67–85. https://doi.org/10.1016/S0048-9697(00)00763-4

Blaauw, M., Christen, J.A., 2005. Radiocarbon peat chronologies and environmental change. J. R. Stat. Soc. Ser. C Appl. Stat. 54, 805–816. https://doi.org/10.1111/j.1467-9876.2005.00516.x

Blaauw, M., Heuvelink, G.B.M., Mauquoy, D., Van Der Plicht, J., Van Geel, B., 2003. A numerical approach to 14C wiggle-match dating of organic deposits: Best fits and confidence intervals. Quat. Sci. Rev. 22, 1485–1500. https://doi.org/10.1016/S0277-3791(03)00086-6

Blaauw, M., van Geel, B., Mauquoy, D., van der Plicht, J., 2004. Carbon-14 wiggle-match dating of peat deposits: Advantages and limitations. J. Quat. Sci. 19, 177–181. https://doi.org/10.1002/jqs.810

Blackford, J.J., 2000. Palaeoclimatic records from peat bogs. Trends Ecol. Evol. 15, 193–198. https://doi.org/10.1016/S0169-5347(00)01826-7

Blockley, S.P.E., Pyne-O'Donnell, S.D.F., Lowe, J.J., Matthews, I.P., Stone, A., Pollard, A.M., Turney, C.S.M., Molyneux, E.G., 2005. A new and less destructive laboratory procedure for the physical separation of distal glass tephra shards from sediments. Quat. Sci. Rev. 24, 1952–1960. https://doi.org/10.1016/j.quascirev.2004.12.008

Booth, R.K., Jackson, S.T., Notaro, M., 2010. Using peatland archives to test paleoclimate hypotheses. PAGES news 18, 1–5.

Bracewell, J.M., Hepburn, A., Thomson, C., 1993. Levels and distribution of polychlorinated biphenyls on the Scottish land mass. Chemosphere 27, 1657–1667. https://doi.org/10.1016/0045-6535(93)90147-W

1053 Brock, F., Lee, S., Housley, R.A., Bronk Ramsey, C., 2011. Variation in the
1054 radiocarbon age of different fractions of peat: A case study from Ahrenshöft,
1055 northern Germany. Quat. Geochronol. 6, 550–555.
1056 https://doi.org/10.1016/j.quageo.2011.08.003

1057 Bronk Ramsey, C., 2013. Recent and Planned Developments of the Program OxCal.
1058 Radiocarbon 55, 720–730. https://doi.org/10.2458/azu_js_rc.55.16215

1059 Bronk Ramsey, C., 2009a. Bayesian Analysis of Radiocarbon Dates. Radiocarbon 51,
1060 337–360. https://doi.org/10.1017/S0033822200033865

1061 Bronk Ramsey, C., 2009b. Dealing with Outliers and Offsets in Radiocarbon Dating.
1062 Radiocarbon 51, 1023–1045. https://doi.org/10.1017/S0033822200034093

1063 Bronk Ramsey, C., 2008. Deposition models for chronological records. Quat. Sci.
1064 Rev. 27, 42–60. https://doi.org/10.1016/j.quascirev.2007.01.019

1065 Campbell, I.D., Campbell, C., Yu, Z., Vitt, D.H., Apps, M.J., 2000. Millennial-Scale
1066 Rhythms in Peatlands in the Western Interior of Canada and in the Global
1067 Carbon Cycle. Quat. Res. 54, 155–158. https://doi.org/10.1006/qres.2000.2134

1068 Certini, G., 2005. Effects of fire on properties of forest soils: A review. Oecologia
1069 143, 1–10. https://doi.org/10.1007/s00442-004-1788-8

1070 Chambers, F.M., Dresser, P.Q., Smith, A.G., 1979. Radiocarbon dating evidence on
1071 the impact of atmospheric pollution on upland peats. Nature 282, 829–831.
1072 https://doi.org/10.1038/282829a0

1073 Charman, D.J., Barber, K.E., Blaauw, M., Langdon, P.G., Mauquoy, D., Daley, T.J.,
1074 Hughes, P.D.M., Karofeld, E., 2009. Climate drivers for peatland palaeoclimate
1075 records. Quat. Sci. Rev. 28, 1811–1819.
1076 https://doi.org/10.1016/j.quascirev.2009.05.013

1077 Charman, D.J., Caseldine, C., Baker, A., Gearey, B., Hatton, J., Proctor, C., 2001.
1078 Paleohydrological Records from Peat Profiles and Speleothems in Sutherland,
1079 Northwest Scotland. Quat. Res. 55, 223–234.
1080 https://doi.org/10.1006/qres.2000.2190

1081 Charman, D.J., Garnett, M.H., 2005. Chronologies for recent peat deposits using
1082 wiggle-matched radiocarbon ages: Problems with old carbon contamination.
1083 Radiocarbon 47, 135–145.

1084 Christen, J.A., Clymo, R.S., Litton, C.D., 1995. A Bayesian Approach to the Use of
1085 14C Dates in the Estimation of the Age of Peat. Radiocarbon 37, 431–441.
1086 https://doi.org/10.1017/S0033822200030915

1087 Clague, J.J., Evans, S.G., Rampton, V.N., Woodsworth, G.J., 1995. Improved age
1088 estimates for the White River and Bridge River tephras, western Canada. Can. J.
1089 Earth Sci. 32, 1172–1179. https://doi.org/10.1139/e95-096

1090 Clymo, R.S., Mackay, D., 1987. Upwash and Downwash of Pollen and Spores in the
1091 Unsaturated Surface Layer of Sphagnum Dominated Peat. New Phytol. 105,
1092 175–183. https://doi.org/10.1111/j.1469-8137.1987.tb00120.x

1093 Clymo, R.S., Oldfield, F., Appleby, P.G., Pearson, G.W., Ratnesar, P., Richardson,
1094 N., 1990. The Record of Atmospheric Deposition on a Rainwater-Dependent
1095 Peatland. Philos. Trans. R. Soc. B Biol. Sci. 327, 331–338.
1096 https://doi.org/10.1098/rstb.1990.0070

Coulter, S.E., Pilcher, J.R., Plunkett, G., Baillie, M., Hall, V.A., Steffensen, J.P., Vinther, B.M., Clausen, H.B., Johnsen, S.J., 2012. Holocene tephras highlight complexity of volcanic signals in Greenland ice cores. J. Geophys. Res. Atmos. 117, 1–11. https://doi.org/10.1029/2012JD017698

Damman, A.W.H., 1978. Distribution and Movement of Elements in Ombrotrophic Peat Bogs. Oikos 30, 480. https://doi.org/10.2307/3543344

Davies, L.J., Froese, D.G., 2015. Developing a cryptotephra framework for North America: A baseline chronostratigraphy for the Holocene from north-western sources., in: XIX INQUA Congress. Nagoya, Japan.

Davies, L.J., Jensen, B.J.L., Froese, D.G., Wallace, K.L., 2016. Late Pleistocene and Holocene tephrostratigraphy of interior Alaska and Yukon: Key beds and chronologies over the past 30,000 years. Quat. Sci. Rev. 146, 28–53. https://doi.org/10.1016/j.quascirev.2016.05.026

Davies, S.M., Elmquist, M., Bergman, J., Wohlfarth, B., Hammarlund, D., 2007. Cryptotephra sedimentation processes within two lacustrine sequences from west central Sweden. The Holocene 17, 319–330. https://doi.org/10.1177/0959683607076443

de Vleeschouwer, F., Fagel, N., Cheburkin, A.K., Pazdur, A., Sikorski, J., Mattielli, N., Renson, V., Fiałkiewicz-Kozieł, B., Piotrowska, N., Le Roux, G., 2009. Anthropogenic impacts in North Poland over the last 1300 years - A record of Pb, Zn, Cu, Ni and S in an ombrotrophic peat bog. Sci. Total Environ. 407, 5674–5684. https://doi.org/10.1016/j.scitotenv.2009.07.020

Degryse, F., Smolders, E., Parker, D.R., 2009. Partitioning of metals (Cd, Co, Cu, Ni, Pb, Zn) in soils: concepts, methodologies, prediction and applications - a review. Eur. J. Soil Sci. 60, 590–612. https://doi.org/10.1111/j.1365-2389.2009.01142.x

Devito, K.J., Mendoza, C., Petrone, R.M., Kettridge, N., Waddington, J.M., 2016. Utikuma Region Study Area (URSA) - Part 1: Hydrogeological and ecohydrological studies (HEAD). For. Chron. 92, 57–61. https://doi.org/10.5558/tfc2016-017

Devito, K.J., Mendoza, C., Qualizza, C., 2012. Conceptualizing water movement in the Boreal Plains: Implications for watershed reconstruction, Canadian Oil Sands Network for Research and Development. Environmental and Reclamation Research Group.

Donovan, J., Kremser, D., Fournelle, J.H., Goemann, K., 2015. Probe for EPMA: Acquisition, automation and analysis.

Dörr, H., 1995. Application of 210Pb in soils. J. Paleolimnol. 13, 157–168. https://doi.org/10.1007/BF00678104

Dreyer, A., Blodau, C., Turunen, J., Radke, M., 2005. The spatial distribution of PAH depositions to peatlands of Eastern Canada. Atmos. Environ. 39, 3725–3733. https://doi.org/10.1016/j.atmosenv.2005.03.009

Dugmore, A.J., Larsen, G., Newton, A.J., 1995. Seven tephra isochrones in Scotland. The Holocene 5, 257–266. https://doi.org/10.1177/095968369500500301

Dugmore, A.J., Newton, A.J., Edwards, K.J., Larsen, G., Blackford, J.J., Cook, G.T., 1996. Long-distance marker horizons from small-scale eruptions: British tephra

deposits from the AD 1510 eruption of Hekla, Iceland. J. Quat. Sci. 11, 511–516. https://doi.org/10.1002/(SICI)1099-1417(199611/12)11:6<511::AID-JQS284>3.0.CO;2-C

El-Daoushy, F., Tolonen, K., Rosenberg, R., 1982. 210 Pb and moss-increment dating of two Finnish Sphagnum hummocks. Nature 296, 429–431. https://doi.org/10.1038/296429a0

Environment and Climate Change Canada, n.d. Canadian Climate Normals. [WWW Document]. URL http://climate.weather.gc.ca/climate_normals/index_e.html (accessed 6.30.17).

Ferraz, M.C.M.A., Lourençlo, J.C.N., 2000. The influence of organic matter content of contaminated soils on the leaching rate of heavy metals. Environ. Prog. 19, 53–58. https://doi.org/10.1002/ep.670190118

Fiałkiewicz-Kozieł, B., Kołaczek, P., Michczyński, A., Piotrowska, N., 2015. The construction of a reliable absolute chronology for the last two millennia in an anthropogenically disturbed peat bog: Limitations and advantages of using a radio-isotopic proxy and age-depth modelling. Quat. Geochronol. 25, 83–95. https://doi.org/10.1016/j.quageo.2014.10.003

Fiałkiewicz-Kozieł, B., Smieja-Król, B., Frontasyeva, M., Słowiński, M., Marcisz, K., Lapshina, E., Gilbert, D., Buttler, A., Jassey, V.E.J., Kaliszan, K., Laggoun-Défarge, F., Kołaczek, P., Lamentowicz, M., 2016. Anthropogenic- and natural sources of dust in peatland during the Anthropocene. Sci. Rep. 6, 38731. https://doi.org/10.1038/srep38731

Franzén, L.G., 2006. Chapter 11 Mineral matter, major elements, and trace elements in raised bog peat: a case study from southern Sweden, Ireland and Tierra del Fuego, south Argentina. Dev. Earth Surf. Process. 9, 241–269. https://doi.org/10.1016/S0928-2025(06)09011-0

Gallagher, D., McGee, E.J., Mitchell, P.I., 2001. A Recent History of 14C, 137Cs, 210Pb, and 241Am Accumulation at Two Irish Peat Bog Sites: an East Versus West Coast Comparison. Radiocarbon 43, 517–525. https://doi.org/10.1017/S0033822200041175

Garnett, M.H., Stevenson, A.C., 2004. Testing the Use of Bomb Radiocarbon to Date the Surface Layers of Blanket Peat. Radiocarbon 46, 841–851. https://doi.org/10.1017/S0033822200035876

Goodsite, M.E., Rom, W., Heinemeier, J., Lange, T., Ooi, S., Appleby, P.G., Shotyk, W., van der Knaap, W.O., Lohse, C., Hansen, T.S., 2001. High-resolution AMS 14C dating of post-bomb peat archives of atmospheric pollutants. Radiocarbon 43, 495–515. https://doi.org/10.1017/S0033822200041163

Goslar, T., Knaap, W.O. Van Der, Hicks, S., Andric, M., Czernik, J., Goslar, E., Rasanen, S., Hyotyla, H., 2005. Radiocarbon dating of modern peat profiles: pre- and post-bomb 14C variations in the construction of age-depth models. Radiocarbon 47, 115–134.

Griggs, A.J., Davies, S.M., Abbott, P.M., Coleman, M., Palmer, A.P., Rasmussen, T.L., Johnston, R., 2015. Visualizing tephra deposits and sedimentary processes in the marine environment: The potential of X-ray microtomography. Geochemistry, Geophys. Geosystems 16, 4329–4343.

https://doi.org/10.1002/2015GC006073

Grybos, M., Davranche, M., Gruau, G., Petitjean, P., 2007. Is trace metal release in wetland soils controlled by organic matter mobility or Fe-oxyhydroxides reduction? J. Colloid Interface Sci. 314, 490–501. https://doi.org/10.1016/j.jcis.2007.04.062

Halsey, L.A., Vitt, D.H., Zoltai, S.C., 1995. Disequilibrium response of permafrost in boreal continental western Canada to climate change. Clim. Change 30, 57–73. https://doi.org/10.1007/BF01093225

Hansson, S. V., Kaste, J.M., Olid, C., Bindler, R., 2014. Incorporation of radiometric tracers in peat and implications for estimating accumulation rates. Sci. Total Environ. 493, 170–177. https://doi.org/10.1016/j.scitotenv.2014.05.088

Hansson, S. V., Tolu, J., Bindler, R., 2015. Downwash of atmospherically deposited trace metals in peat and the influence of rainfall intensity: An experimental test. Sci. Total Environ. 506–507, 95–101. https://doi.org/10.1016/j.scitotenv.2014.10.083

He, Q., Walling, D.E., 1996. Interpreting particle size effects in the adsorption of 137Cs and unsupported 210Pb by mineral soils and sediments. J. Environ. Radioact. 30, 117–137. https://doi.org/10.1016/0265-931X(96)89275-7

Holmquist, J.R., Finkelstein, S.A., Garneau, M., Massa, C., Yu, Z., MacDonald, G.M., 2016. A comparison of radiocarbon ages derived from bulk peat and selected plant macrofossils in basal peat cores from circum-arctic peatlands. Quat. Geochronol. 31, 53–61. https://doi.org/10.1016/j.quageo.2015.10.003

Hua, Q., Barbetti, M., Rakowski, A.Z., 2013. Atmospheric radiocarbon for the period 1950-2010. Radiocarbon 55, 2059–2072. https://doi.org/10.2458/azu_js_rc.v55i2.16177

Ingram, H.A.P., 1978. Soil Layers in Mires: Function and Terminology. J. Soil Sci. 29, 224–227. https://doi.org/10.1111/j.1365-2389.1978.tb02053.x

Jensen, B.J.L., Beaudoin, A.B., 2016. Geochemical characterization of tephra deposits at archaeological and palaeoenvironmental sites across south-central Alberta and southwest Saskatchewan, in: Woywitka, R. (Ed.), Back on the Horse: Recent Developments in Archaeological and Palaeontological Research in Alberta. Archaeological Survey of Alberta, Edmonton, Alberta, pp. 154–160.

Jensen, B.J.L., Froese, D.G., Preece, S.J., Westgate, J.A., Stachel, T., 2008. An extensive middle to late Pleistocene tephrochronologic record from east-central Alaska. Quat. Sci. Rev. 27, 411–427. https://doi.org/10.1016/j.quascirev.2007.10.010

Jensen, B.J.L., Pyne-O'Donnell, S., Plunkett, G., Froese, D.G., Hughes, P.D.M., Sigl, M., McConnell, J.R., Amesbury, M.J., Blackwell, P.G., van den Bogaard, C., Buck, C.E., Charman, D.J., Clague, J.J., Hall, V.A., Koch, J., Mackay, H., Mallon, G., McColl, L., Pilcher, J.R., 2014. Transatlantic distribution of the Alaskan White River Ash. Geology 42, 875–878. https://doi.org/10.1130/G35945.1

Jones, J.M., Hao, J., 1993. Ombrotrophic peat as a medium for historical monitoring of heavy metal pollution. Environ. Geochem. Health 15, 67–74. https://doi.org/10.1007/BF02627824

1231 Kilian, M.R., Van der Plicht, J., Van Geel, B., 1995. Dating raised bogs: New aspects
1232 of AMS 14C wiggle matching, a reservoir effect and climatic change. Quat. Sci.
1233 Rev. 14, 959–966. https://doi.org/10.1016/0277-3791(95)00081-X

1234 Kuehn, S.C., Froese, D.G., Carrara, P.E., Foit, F.F., Pearce, N.J.G., Rotheisler, P.,
1235 2009. Major- and trace-element characterization, expanded distribution, and a
1236 new chronology for the latest Pleistocene Glacier Peak tephras in western North
1237 America. Quat. Res. 71, 201–216. https://doi.org/10.1016/j.yqres.2008.11.003

1238 Kuehn, S.C., Froese, D.G., Shane, P.A.R., 2011. The INTAV intercomparison of
1239 electron-beam microanalysis of glass by tephrochronology laboratories: Results
1240 and recommendations. Quat. Int. 246, 19–47.
1241 https://doi.org/10.1016/j.quaint.2011.08.022

1242 Lamborg, C.H., Fitzgerald, W.F., Damman, A.W.H., Benoit, J.M., Balcom, P.H.,
1243 Engstrom, D.R., 2002. Modern and historic atmospheric mercury fluxes in both
1244 hemispheres: Global and regional mercury cycling implications. Global
1245 Biogeochem. Cycles 16, 51-1-51–11. https://doi.org/10.1029/2001GB001847

1246 Le Roux, G., Aubert, D., Stille, P., Krachler, M., Kober, B., Cheburkin, A., Bonani,
1247 G., Shotyk, W., 2005. Recent atmospheric Pb deposition at a rural site in
1248 southern Germany assessed using a peat core and snowpack, and comparison
1249 with other archives. Atmos. Environ. 39, 6790–6801.
1250 https://doi.org/10.1016/j.atmosenv.2005.07.026

1251 Le Roux, G., Fagel, N., de Vleeschouwer, F., Krachler, M., Debaille, V., Stille, P.,
1252 Mattielli, N., van der Knaap, W.O., van Leeuwen, J.F.N., Shotyk, W., 2012.
1253 Volcano- and climate-driven changes in atmospheric dust sources and fluxes
1254 since the late glacial in Central Europe. Geology 40, 335–338.
1255 https://doi.org/10.1130/G32586.1

1256 Le Roux, G., Marshall, W.A., 2011. Constructing recent peat accumulation
1257 chronologies using atmospheric fall-out radionuclides. Mires Peat 7, 1–14.

1258 Litton, C.D., Buck, C.E., 1995. The Bayesian Approach To the Interpretation of
1259 Archaeological Data. Archaeometry 37, 1–24. https://doi.org/10.1111/j.1475-
1260 4754.1995.tb00723.x

1261 Łokas, E., Mietelski, J.W., Ketterer, M.E., Kleszcz, K., Wachniew, P., Michalska, S.,
1262 Miecznik, M., 2013. Sources and vertical distribution of 137Cs, 238Pu,
1263 239+240Pu and 241Am in peat profiles from southwest Spitsbergen. Appl.
1264 Geochemistry 28, 100–108. https://doi.org/10.1016/j.apgeochem.2012.10.027

1265 Lowe, D.J., Blaauw, M., Hogg, A.G., Newnham, R.M., 2013. Ages of 24 widespread
1266 tephras erupted since 30,000 years ago in New Zealand, with re-evaluation of the
1267 timing and palaeoclimatic implications of the Lateglacial cool episode recorded
1268 at Kaipo bog. Quat. Sci. Rev. 74, 170–194.
1269 https://doi.org/10.1016/j.quascirev.2012.11.022

1270 Lusa, M., Bomberg, M., Virtanen, S., Lempinen, J., Aromaa, H., Knuutinen, J., Lehto,
1271 J., 2015. Factors affecting the sorption of cesium in a nutrient-poor boreal bog. J.
1272 Environ. Radioact. 147, 22–32. https://doi.org/10.1016/j.jenvrad.2015.05.005

1273 Mackay, H., Hughes, P.D.M., Jensen, B.J.L., Langdon, P.G., Pyne-O'Donnell, S.D.F.,
1274 Plunkett, G., Froese, D.G., Coulter, S.E., Gardner, J.E., 2016. A mid to late
1275 Holocene cryptotephra framework from eastern North America. Quat. Sci. Rev.

132, 101–113. https://doi.org/10.1016/j.quascirev.2015.11.011

MacKenzie, A.B., Farmer, J.G., Sugden, C.L., 1997. Isotopic evidence of the relative retention and mobility of lead and radiocaesium in Scottish ombrotrophic peats. Sci. Total Environ. 203, 115–127. https://doi.org/10.1016/S0048-9697(97)00139-3

Magnan, G., van Bellen, S., Davies, L., Froese, D., Garneau, M., Mullan-Boudreau, G., Zaccone, C., Shotyk, W., 2018. Impact of the Little Ice Age cooling and 20th century climate change on peatland vegetation dynamics in central and northern Alberta using a multi-proxy approach and high-resolution peat chronologies. Quat. Sci. Rev. 185, 230–243. https://doi.org/10.1016/j.quascirev.2018.01.015

Martínez, C.E., McBride, M.B., 1999. Dissolved and labile concentrations of Cd, Cu, Pb, and Zn in aged ferrihydrite - Organic matter systems. Environ. Sci. Technol. 33, 745–750. https://doi.org/10.1021/es980576c

Miller, T.P., McGimsey, R.G., Richter, D.H., Riehle, J.R., Nye, G.J., Yount, M.E., Dumoulin, J.A., 1998. Catalog of the historically active volcanoes of Alaska (No. 98–582), Open-File Report. U.S. Dept. of the Interior, U.S. Geological Survey.

Morgan, G.B., London, D., 2005. Effect of current density on the electron microprobe analysis of alkali aluminosilicate glasses. Am. Mineral. 90, 1131–1138. https://doi.org/10.2138/am.2005.1769

Mullan-Boudreau, G., Belland, R., Devito, K.J., Noernberg, T., Pelletier, R., Shotyk, W., 2017. Sphagnum Moss as an Indicator of Contemporary Rates of Atmospheric Dust Deposition in the Athabasca Bituminous Sands Region. Environ. Sci. Technol. 51, 7422–7431. https://doi.org/10.1021/acs.est.6b06195

Mullineaux, D., 1996. Pre-1980 tephra-fall deposits erupted from Mount St. Helens, Washington. (No. 1563), Professional Paper.

Nielsen, C.H., Sigurdsson, H., 1981. Quantitative methods for electron microprobe analysis of sodium in natural and synthetic glasses. Am. Mineral. 66, 547–552.

Nilsson, M., Klarqvist, M., Possnert, G., 2001. Variation in 14C age of macrofossils and different fractions of minute peat samples dated by AMS. The Holocene 11, 579–586. https://doi.org/10.1191/095968301680223521

Novák, M., Zemanova, L., Voldrichova, P., Stepanova, M., Adamova, M., Pacherova, P., Komarek, A., Krachler, M., Prechova, E., 2011. Experimental evidence for mobility/immobility of metals in peat. Environ. Sci. Technol. 45, 7180–7187. https://doi.org/10.1021/es201086v

Oldfield, F., Appleby, P.G., Cambray, R.S., Eakins, J.D., Barber, K.E., Battarbee, R.W., Pearson, G.R., Williams, J.M., 1979. 210 Pb, 137 Cs and 239 Pu Profiles in Ombrotrophic Peat. Oikos 33, 40. https://doi.org/10.2307/3544509

Oldfield, F., Richardson, N., Appleby, P.G., 1995. Radiometric dating (210Pb, 137Cs, 241Am) of recent ombrotrophic peat accumulation and evidence for changes in mass balance. The Holocene 5, 141–148. https://doi.org/10.1177/095968369500500202

Oldfield, F., Thompson, R., Crooks, P.R.J., Gedye, S.J., Hall, V.A., Harkness, D.D., Housley, R. a., McCormac, F.G., Newton, A.J., Pilcher, J.R., Renberg, I.,

Richardson, N., 1997. Radiocarbon dating of a recent high latitude peat profile: Stor Åmyran, northern Sweden. The Holocene 7, 283–290. https://doi.org/10.1177/095968369700700304

Oldfield, F., Tolonen, K., Thompson, R., 1981. History of particulate atmospheric pollution from magnetic measurements in dated Finnish peat profiles. Ambio 10, 185–188.

Olid, C., Diego, D., Garcia-Orellana, J., Cortizas, A.M., Klaminder, J., 2016. Modeling the downward transport of 210Pb in Peatlands: Initial Penetration-Constant Rate of Supply (IP-CRS) model. Sci. Total Environ. 541, 1222–1231. https://doi.org/10.1016/j.scitotenv.2015.09.131

Osborn, G., 1985. Holocene tephrostratigraphy and glacial fluctuations in Waterton Lakes and Glacier national parks, Alberta and Montana. Can. J. Earth Sci. 22, 1093–1101. https://doi.org/10.1139/e85-111

Parry, L.E., Charman, D.J., Blake, W.H., 2013. Comparative dating of recent peat deposits using natural and anthropogenic fallout radionuclides and Spheroidal Carbonaceous Particles (SCPs) at a local and landscape scale. Quat. Geochronol. 15, 11–19. https://doi.org/10.1016/j.quageo.2013.01.002

Payne, R., Blackford, J., van der Plicht, J., 2008. Using cryptotephras to extend regional tephrochronologies: An example from southeast Alaska and implications for hazard assessment. Quat. Res. 69, 42–55. https://doi.org/10.1016/j.yqres.2007.10.007

Payne, R.J., Gehrels, M., 2010. The formation of tephra layers in peatlands: An experimental approach. Catena 81, 12–23. https://doi.org/10.1016/j.catena.2009.12.001

Payne, R.J., Kilfeather, A.A., van der Meer, J.J.M., Blackford, J.J., 2005. Experiments on the taphonomy of tephra in peat. Suo 56, 147–156.

Petrone, R.M., Devito, K.J., Mendoza, C., 2016. Utikuma Region Study Area (URSA) - Part 2: Aspen Harvest and Recovery Study. For. Chron. 92, 62–65. https://doi.org/10.5558/tfc2016-018

Péwé, T.L., 1975. Quaternary Geology of Alaska. U.S. Geol. Surv. Prof. Pap., Geological Survery Professional Paper 835.

Pilcher, J.R., Hall, V.A., McCormac, F.G., 1995. Dates of Holocene Icelandic volcanic eruptions from tephra layers in Irish peats. The Holocene 5, 103–110. https://doi.org/10.1177/095968369500500111

Piotrowska, N., Blaauw, M., Mauquoy, D., Chambers, F.M., 2011. Constructing deposition chronologies for peat deposits using radiocarbon dating. Mires Peat 7, 1–14.

Piotrowska, N., De Vleeschouwer, F., Sikorski, J., Pawlyta, J., Fagel, N., Le Roux, G., Pazdur, A., 2010. Intercomparison of radiocarbon bomb pulse and 210Pb age models. A study in a peat bog core from North Poland. Nucl. Instruments Methods Phys. Res. Sect. B Beam Interact. with Mater. Atoms 268, 1163–1166. https://doi.org/10.1016/j.nimb.2009.10.124

Plunkett, G., 2006. Tephra-linked peat humification records from Irish ombrotrophic bogs question nature of solar forcing at 850 cal. yr BC. J. Quat. Sci. 21, 9–16.

https://doi.org/10.1002/jqs.951

Pratte, S., Mucci, A., Garneau, M., 2013. Historical records of atmospheric metal deposition along the St. Lawrence Valley (eastern Canada) based on peat bog cores. Atmos. Environ. 79, 831–840. https://doi.org/10.1016/j.atmosenv.2013.07.063

Pyne-O'Donnell, S.D.F., 2011. The taphonomy of Last Glacial-Interglacial Transition (LGIT) distal volcanic ash in small Scottish lakes. Boreas 40, 131–145. https://doi.org/10.1111/j.1502-3885.2010.00154.x

Pyne-O'Donnell, S.D.F., Hughes, P.D.M., Froese, D.G., Jensen, B.J.L., Kuehn, S.C., Mallon, G., Amesbury, M.J., Charman, D.J., Daley, T.J., Loader, N.J., Mauquoy, D., Street-Perrott, F.A., Woodman-Ralph, J., 2012. High-precision ultra-distal Holocene tephrochronology in North America. Quat. Sci. Rev. 52, 6–11. https://doi.org/10.1016/j.quascirev.2012.07.024

Rausch, N., Nieminen, T., Ukonmaanaho, L., Le Roux, G., Krachler, M., Cheburkin, A.K., Bonani, G., Shotyk, W., 2005. Comparison of atmospheric deposition of copper, nickel, cobalt, zinc, and cadmium recorded by Finnish peat cores with monitoring data and emission records. Environ. Sci. Technol. 39, 5989–5998. https://doi.org/10.1021/es050260m

Reimer, P.J., Bard, E., Bayliss, A., Beck, J.W., Blackwell, P.G., Bronk Ramsey, C., Buck, C.E., Cheng, H., Edwards, R.L., Friedrich, M., Grootes, P.M., Guilderson, T.P., Haflidason, H., Hajdas, I., Hatté, C., Heaton, T.J., Hoffmann, D.L., Hogg, A.G., Hughen, K.A., Kaiser, K.F., Kromer, B., Manning, S.W., Niu, M., Reimer, R.W., Richards, D.A., Scott, E.M., Southon, J.R., Staff, R.A., Turney, C.S.M., van der Plicht, J., 2013. IntCal13 and Marine13 Radiocarbon Age Calibration Curves 0–50,000 Years cal BP. Radiocarbon 55, 1869–1887. https://doi.org/10.2458/azu_js_rc.55.16947

Reyes, A. V., Jensen, B.J.L., Zazula, G.D., Ager, T.A., Kuzmina, S., La Farge, C., Froese, D.G., 2010. A late-Middle Pleistocene (Marine Isotope Stage 6) vegetated surface buried by Old Crow tephra at the Palisades, interior Alaska. Quat. Sci. Rev. 29, 801–811. https://doi.org/10.1016/j.quascirev.2009.12.003

Robinson, S.D., Turetsky, M.R., Kettles, I.M., Wieder, R.K., 2003. Permafrost and peatland carbon sink capacity with increasing latitude, in: Phillips, M., Springman, S., Arenson, L. (Eds.), Proceedings of the 8th International Conference on Permafrost. Balkema Publishers, Zurich, pp. 965–970.

Roland, T.P., Mackay, H., Hughes, P.D.M., 2015. Tephra analysis in ombrotrophic peatlands: A geochemical comparison of acid digestion and density separation techniques. J. Quat. Sci. 30, 3–8. https://doi.org/10.1002/jqs.2754

Roos-Barraclough, F., Martinez-Cortizas, A., Garcia-Rodeja, E., Shotyk, W., 2002. A 14 500 year record of the accumulation of atmospheric mercury in peat: Volcanic signals, anthropogenic influences and a correlation to bromine accumulation. Earth Planet. Sci. Lett. 202, 435–451. https://doi.org/10.1016/S0012-821X(02)00805-1

Roos-Barraclough, F., Shotyk, W., 2003. Millennial-scale records of atmospheric mercury deposition obtained from ombrotrophic and minerotrophic peatlands in the Swiss Jura mountains. Environ. Sci. Technol. 37, 235–244. https://doi.org/10.1021/es0201496

Sanchez-Cabeza, J.A., Ruiz-Fernández, A.C., 2012. 210Pb sediment radiochronology: An integrated formulation and classification of dating models. Geochim. Cosmochim. Acta 82, 183–200. https://doi.org/10.1016/j.gca.2010.12.024

Sanders, G., Jones, K.C., Hamilton-Taylor, J., Dorr, H., 1995. PCB and PAH fluxes to a dated UK peat core. Environ. Pollut. 89, 17–25. https://doi.org/10.1016/0269-7491(94)00048-I

Sapkota, A., Cheburkin, A.K., Bonani, G., Shotyk, W., 2007. Six millennia of atmospheric dust deposition in southern South America (Isla Navarino, Chile). The Holocene 17, 561–572. https://doi.org/10.1177/0959683607078981

Schell, W.R., Tobin, M.J., Massey, C.D., 1989. Evaluation of trace metal deposition history and potential element mobility in selected cores from peat and wetland ecosystems. Sci. Total Environ. 87–88, 19–42. https://doi.org/10.1016/0048-9697(89)90223-4

Schleich, N., Degering, D., Unterricker, S., 2000. Natural and artificial radionuclides in forest and bog soils: Tracers for migration processes and soil development. Radiochim. Acta 88, 803–808. https://doi.org/10.1524/ract.2000.88.9-11.803

Schoning, K., Charman, D.J., Wastegård, S., 2005. Reconstructed water tables from two ombrotrophic mires in eastern central Sweden compared with instrumental meteorological data. The Holocene 15, 111–118. https://doi.org/10.1191/0959683605hl772rp

Shore, J.S., Bartley, D.D., Harkness, D.D., 1995. Problems encountered with the 14C dating of peat. Quat. Sci. Rev. 14, 373–383. https://doi.org/10.1016/0277-3791(95)00031-3

Shotyk, W., 1996. Peat bog archives of atmospheric metal deposition: geochemical evaluation of peat profiles, natural variations in metal concentrations, and metal enrichment factors. Environ. Rev. 4, 149–183. https://doi.org/10.1139/a96-010

Shotyk, W., Appleby, P.G., Bicalho, B., Davies, L.J., Froese, D.G., Grant-Weaver, I., Krachler, M., Magnan, G., Mullan-Boudreau, G., Noernberg, T., Pelletier, R., Shannon, B., van Bellen, S., Zaccone, C., 2016a. Peat bogs in northern Alberta, Canada reveal decades of declining atmospheric Pb contamination. Geophys. Res. Lett. 43, 9964–9974. https://doi.org/10.1002/2016GL070952

Shotyk, W., Appleby, P.G., Bicalho, B., Davies, L.J., Froese, D.G., Grant-Weaver, I., Magnan, G., Mullan-Boudreau, G., Noernberg, T., Pelletier, R., Shannon, B., van Bellen, S., Zaccone, C., 2017. Peat Bogs Document Decades of Declining Atmospheric Contamination by Trace Metals in the Athabasca Bituminous Sands Region. Environ. Sci. Technol. 51, 6237–6249. https://doi.org/10.1021/acs.est.6b04909

Shotyk, W., Cheburkin, A.K., Appleby, P.G., Fankhauser, A., Kramers, J.D., 1997. Lead in three peat bog profiles, Jura Mountains, Switzerland: Enrichment factors, isotopic composition, and chronology of atmospheric deposition. Water. Air. Soil Pollut. 100, 297–310. https://doi.org/10.1023/A:1018384711802

Shotyk, W., Kempter, H., Krachler, M., Zaccone, C., 2015. Stable (^{206}Pb, ^{207}Pb, ^{208}Pb) and radioactive (^{210}Pb) lead isotopes in 1year of growth of Sphagnum moss from four ombrotrophic bogs in southern Germany: Geochemical significance and environmental implications. Geochim. Cosmochim. Acta 163, 101–125.

https://doi.org/10.1016/j.gca.2015.04.026

Shotyk, W., Rausch, N., Outridge, P.M., Krachler, M., 2016b. Isotopic evolution of atmospheric Pb from metallurgical processing in Flin Flon, Manitoba: Retrospective analysis using peat cores from bogs. Environ. Pollut. 218, 338–348. https://doi.org/10.1016/j.envpol.2016.07.009

Shotyk, W., Wayne Nesbitt, H., Fyfe, W.S., 1992. Natural and antropogenic enrichments of trace metals in peat profiles. Int. J. Coal Geol. 20, 49–84. https://doi.org/10.1016/0166-5162(92)90004-G

Smith, J.T., Appleby, P.G., Hilton, J., Richardson, N., 1997. Inventories and fluxes of 210Pb, 137Cs and 241Am determined from the soils of three small catchments in Cumbria, UK. J. Environ. Radioact. 37, 127–142. https://doi.org/10.1016/S0265-931X(97)00003-9

Sokolik, G., Ovsiannikova, S., Kimlenko, I., 2002. Distribution and mobility of 137 Cs, 90 Sr, 239,240 Pu and 241 Am in solid phase-interstitial soil solution system. Radioprotection 37, C1-259-C1-264. https://doi.org/10.1051/radiopro/2002048

Spray, J.G., Rae, D.A., 1995. Quantitative electron-microprobe analysis of alkali silicate glasses: a review and user guide. Can. Mineral. 33, 323–332.

Strawn, D.G., Sparks, D.L., 2000. Effects of Soil Organic Matter on the Kinetics and Mechanisms of Pb(II) Sorption and Desorption in Soil. Soil Sci. Soc. Am. J. 64, 144. https://doi.org/10.2136/sssaj2000.641144x

Swindles, G.T., De Vleeschouwer, F., Plunkett, G., 2010. Dating peat profiles using tephra: stratigraphy, geochemistry and chronology. Mires Peat 7, 1–9.

Swindles, G.T., Galloway, J.M., Outram, Z., Turner, K., Schofield, J.E., Newton, A.J., Dugmore, A.J., Church, M.J., Watson, E.J., Batt, C., Bond, J., Edwards, K.J., Turner, V., Bashford, D., 2013. Re-deposited cryptotephra layers in Holocene peats linked to anthropogenic activity. The Holocene 23, 1493–1501. https://doi.org/10.1177/0959683613489586

Swindles, G.T., Patterson, R.T., Roe, H.M., Galloway, J.M., 2012. Evaluating periodicities in peat-based climate proxy records. Quat. Sci. Rev. 41, 94–103. https://doi.org/10.1016/j.quascirev.2012.03.003

Syrovetnik, K., Malmström, M.E., Neretnieks, I., 2007. Accumulation of heavy metals in the Oostriku peat bog, Estonia: Determination of binding processes by means of sequential leaching. Environ. Pollut. 147, 291–300. https://doi.org/10.1016/j.envpol.2005.10.048

Testa, C., Jia, G., Degetto, S., Desideri, D., Guerra, F., Meli, M.A., Roselli, C., 1999. Vertical profiles of 239,240Pu and 241Am in two sphagnum mosses of Italian peat. Sci. Total Environ. 232, 27–31. https://doi.org/10.1016/S0048-9697(99)00106-0

Toohey, M., Sigl, M., 2017. Volcanic stratospheric sulfur injections and aerosol optical depth from 500 BCE to 1900 CE. Earth Syst. Sci. Data 9, 809–831. https://doi.org/10.5194/essd-9-809-2017

Treat, C.C., Jones, M.C., Camill, P., Gallego-Sala, A., Garneau, M., Harden, J.W., Hugelius, G., Klein, E.S., Kokfelt, U., Kuhry, P., Loisel, J., Mathijssen, P.J.H., O'Donnell, J.A., Oksanen, P.O., Ronkainen, T.M., Sannel, A.B.K., Talbot, J.,

Tarnocai, C., Väliranta, M., 2016. Effects of permafrost aggradation on peat properties as determined from a pan-Arctic synthesis of plant macrofossils. J. Geophys. Res. G Biogeosciences 121, 78–94. https://doi.org/10.1002/2015JG003061

Trivedi, P., Dyer, J.A., Sparks, D.L., 2003. Lead sorption onto ferrihydrite. 1. A macroscopic and spectroscopic assessment. Environ. Sci. Technol. 37, 908–914. https://doi.org/10.1021/es0257927

Turetsky, M.R., Manning, S.W., Wieder, R.K., 2004. Dating recent peat deposits. Wetlands 24, 324–356. https://doi.org/10.1672/0277-5212(2004)024[0324:DRPD]2.0.CO;2

Turetsky, M.R., Wieder, R.K., Vitt, D.H., Evans, R.J., Scott, K.D., 2007. The disappearance of relict permafrost in boreal north America: Effects on peatland carbon storage and fluxes. Glob. Chang. Biol. 13, 1922–1934. https://doi.org/10.1111/j.1365-2486.2007.01381.x

Turetsky, M.R., Wieder, R.K., Williams, C.J., Vitt, D.H., 2000. Organic Matter Accumulation, Peat Chemistry, and Permafrost Melting in Peatlands of Boreal Alberta. Ecoscience 7, 379–392. https://doi.org/10.1080/11956860.2000.11682608

Tylmann, W., Bonk, A., Goslar, T., Wulf, S., Grosjean, M., 2016. Calibrating 210Pb dating results with varve chronology and independent chronostratigraphic markers: Problems and implications. Quat. Geochronol. 32, 1–10. https://doi.org/10.1016/j.quageo.2015.11.004

Urban, N.R., Eisenreich, S.J., Grigal, D.F., Schurr, K.T., 1990. Mobility and diagenesis of Pb and 210Pb in peat. Geochim. Cosmochim. Acta 54, 3329–3346. https://doi.org/10.1016/0016-7037(90)90288-V

van Bellen, S., Magnan, G., Davies, L., Froese, D., Mullan-Boudreau, G., Zaccone, C., Garneau, M., Shotyk, W., 2018. Testate amoeba records indicate regional 20 th -century lowering of water tables in ombrotrophic peatlands in central-northern Alberta, Canada. Glob. Chang. Biol. https://doi.org/10.1111/gcb.14143

van der Linden, M., Vickery, E., Charman, D.J., van Geel, B., 2008. Effects of human impact and climate change during the last 350 years recorded in a Swedish raised bog deposit. Palaeogeogr. Palaeoclimatol. Palaeoecol. 262, 1–31. https://doi.org/10.1016/j.palaeo.2008.01.018

van der Plicht, J., Yeloff, D., van der Linden, M., van Geel, B., Brain, S., Chambers, F.M., Webb, J., Toms, P., 2013. Dating recent peat accumulation in European ombrotrophic bogs. Radiocarbon 55, 1763–1778. https://doi.org/10.2458/azu_js_rc.55.16057

van Geel, B., Mook, W.G., 1989. High-resolution 14C dating of organic deposits using natural atmospheric 14C variations. Radiocarbon 31, 151–155. https://doi.org/10.1017/S0033822200044805

van Hoof, P.L., Andren, A.W., 1989. Partitioning and Transport of 210Pb in Lake Michigan. J. Great Lakes Res. 15, 498–509. https://doi.org/10.1016/S0380-1330(89)71505-7

Vile, M.A., Wieder, R.K., Novák, M., 1999. Mobility of Pb in Sphagnum-derived peat. Biogeochemistry 45, 35–52. https://doi.org/10.1023/A:1006085410886

Vitt, D.H., Halsey, L.A., Zoltai, S.C., 2000. The changing landscape of Canada's western boreal forest: the current dynamics of permafrost. Can. J. For. Res. 30, 283–287. https://doi.org/10.1139/x99-214

Vitt, D.H., Halsey, L.A., Zoltai, S.C., 1994. The bog landforms of continental Western Canada in relation to climate and permafrost patterns. Arct. Alp. Res. 26, 1–13. https://doi.org/10.2307/1551870

Watson, E.J., Swindles, G.T., Lawson, I.T., Savov, I., 2015. Spatial variability of tephra and carbon accumulation in a Holocene peatland. Quat. Sci. Rev. 124, 248–264. https://doi.org/10.1016/j.quascirev.2015.07.025

Watson, E.J., Swindles, G.T., Lawson, I.T., Savov, I.P., 2016. Do peatlands or lakes provide the most comprehensive distal tephra records? Quat. Sci. Rev. 139, 110–128. https://doi.org/10.1016/j.quascirev.2016.03.011

Weiss, D., Shotyk, W., Kramers, J.D., Gloor, M., 1999. Sphagnum mosses as archives of recent and past atmospheric lead deposition in Switzerland. Atmos. Environ. 33, 3751–3763. https://doi.org/10.1016/S1352-2310(99)00093-X

Westgate, J.A., Smith, D., Nichols, H., 1969. Late Quaternary pyroclastic layers in the Edmonton area, Alberta., in: Pawluk, S. (Ed.), Proceedings of Symposium on Pedology and Quaternary Research, Geology Department Contract. Edmonton, Alberta, pp. 180–186.

Westgate, J.A., Smith, D., Tomlinson, M., 1970. Late Quaternary tephra layers in southwestern Canada, in: Smith, R.A., Smith, J.W. (Eds.), Early Man and Environments in Northwest North America. Calgary, Alberta, pp. 13–34.

Wieder, R.K., Novák, M., Schell, W.R., Rhodes, T., 1994. Rates of peat accumulation over the past 200 years in five Sphagnum-dominated peatlands in the United States. J. Paleolimnol. 12, 35–47. https://doi.org/10.1007/BF00677988

Wieder, R.K., Vile, M.A., Albright, C.M., Scott, K.D., Vitt, D.H., Quinn, J.C., Burke-Scoll, M., 2016. Effects of altered atmospheric nutrient deposition from Alberta oil sands development on Sphagnum fuscum growth and C, N and S accumulation in peat. Biogeochemistry 129, 1–19. https://doi.org/10.1007/s10533-016-0216-6

Yamaguchi, D.K., Hoblitt, R.P., 1995. Tree-ring dating of pre-1980 volcanic flowage deposits at Mount St. Helens, Washington. Geol. Soc. Am. Bull. 107, 1077–1093. https://doi.org/10.1130/0016-7606(1995)107<1077:TRDOPV>2.3.CO;2

Yang, H., Rose, N.L., Boyle, J.F., Battarbee, R.W., 2001. Storage and distribution of trace metals and spheroidal carbonaceous particles (SCPs) from atmospheric deposition in the catchment peats of Lochnagar, Scotland. Environ. Pollut. 115, 231–238. https://doi.org/10.1016/S0269-7491(01)00107-5

Yeloff, D., Bennett, K.D., Blaauw, M., Mauquoy, D., Sillasoo, Ü., van der Plicht, J., van Geel, B., 2006. High precision 14C dating of Holocene peat deposits: A comparison of Bayesian calibration and wiggle-matching approaches. Quat. Geochronol. 1, 222–235. https://doi.org/10.1016/j.quageo.2006.08.003

Yu, Z., Vitt, D.H., Campbell, I.D., Apps, M.J., 2003. Understanding Holocene peat accumulation pattern of continental fens in western Canada. Can. J. Bot. 81, 267–282. https://doi.org/10.1139/b03-016

1588 Zaccone, C., Cocozza, C., Cheburkin, A.K., Shotyk, W., Miano, T.M., 2008.
1589 Distribution of As, Cr, Ni, Rb, Ti and Zr between peat and its humic fraction
1590 along an undisturbed ombrotrophic bog profile (NW Switzerland). Appl.
1591 Geochemistry 23, 25–33. https://doi.org/10.1016/j.apgeochem.2007.09.002

1592 Zaccone, C., Cocozza, C., Cheburkin, A.K., Shotyk, W., Miano, T.M., 2007. Highly
1593 organic soils as "witnesses" of anthropogenic Pb, Cu, Zn, and 137Cs inputs
1594 during centuries. Water. Air. Soil Pollut. 186, 263–271.
1595 https://doi.org/10.1007/s11270-007-9482-1

1596 Zaretskaia, N.E., Ponomareva, V. V, Sulerzhitsky, L.D., Zhilin, M.G., 2001.
1597 Radiocarbon Studies of Peat Bogs: an Investigation of South Kamchatka
1598 Volcanoes and Upper Volga Archeological Sites. Radiocarbon 43, 571–580.
1599 https://doi.org/10.1017/S0033822200041229

1600 Zhang, Y., Shotyk, W., Zaccone, C., Noernberg, T., Pelletier, R., Bicalho, B., Froese,
1601 D.G., Davies, L.J., Martin, J.W., 2016. Airborne Petcoke Dust is a Major Source
1602 of Polycyclic Aromatic Hydrocarbons in the Athabasca Oil Sands Region.
1603 Environ. Sci. Technol. 50, 1711–1720. https://doi.org/10.1021/acs.est.5b05092

1604 Zhao, Y., Hölzer, A., Yu, Z., 2007. Late Holocene Natural and Human-Induced
1605 Environmental Change Reconstructed from Peat Records in Eastern Central
1606 China. Radiocarbon 49, 789–798. https://doi.org/10.1017/S0033822200042661

1607 Zoltai, S.C., 1995. Permafrost Distribution in Peatlands of West-Central Canada
1608 during the Holocene Warm Period 6000 Years BP. Geogr. Phys. Quat. 49, 45–
1609 54. https://doi.org/10.7202/033029ar

1610 Zoltai, S.C., 1993. Cyclic Development of Permafrost in the Peatlands of
1611 Northwestern Canada. Arct. Alp. Res. 25, 240–246.
1612 https://doi.org/10.2307/1551820

1613 Zoltai, S.C., 1989. Late Quaternary volcanic ash in the peatlands of central Alberta.
1614 Can. J. Earth Sci. 26, 207–214. https://doi.org/10.1139/e89-017

1615 Zoltai, S.C., Tarnocai, C., 1975. Perennially Frozen Peatlands in the Western Arctic
1616 and Subarctic of Canada. Can. J. Earth Sci. 12, 28–43.
1617 https://doi.org/10.1139/e75-004

1618 Zoltai, S.C., Vitt, D.H., 1990. Holocene climatic change and the distribution of
1619 peatlands in western interior Canada. Quat. Res. 33, 231–240.
1620 https://doi.org/10.1016/0033-5894(90)90021-C

1621

Tables

Table 1: Event histories for the cores analysed from each site, including the depth of the inferred changes and the proxy data used to support this. Events included in the final age models as boudnaries are shown with a Y; those not included are shown with an N. WTD = water table depth; C/N and H/C refer to measurements of isotopic ratios.

Site	Boundary depth	Proxy information	Event	In model?
ANZ	24.67	S. Fuscum established		Y
	30.28	WTD, H/C	Permafrost thaw	Y
	36.59-40.75	WTD, H/C, charcoal >1mm, charred needles	Permafrost aggradation and fire	Y/Y
	61.36	Charcoal >1mm, charred needles	Local fire	Y
	69.62	Charred needles, some charcoal >1mm	Local fire	N
	86.36	Charcoal >1mm	Possible fire	N
JPH	0-5.24	WTD, Picea needles	Dry conditions, Picea trees	Y
	12.89	S. Acutfolia established		Y
	28.65-32.75	Charcoal >1mm, charred macros, WTD	Dry phase, local fires	N/N
	36.77	Charcoal >1mm, charred macros	Local fire	Y
	51.22	Cyperaceae, C/N	Wet to dry transition	Y
McK	27.46-31.96	Polytrichum	Drying	Y/Y
	41.18	WTD, Polytrichum	Wet to dry shift	Y
	45.92-57.9	Charcoal >1mm, charred needles	Multiple local fires	N/Y
	77.08-82.29	Charcoal >1mm, charred needles	Local fires	N/N
McM	19.61	S. Acutfolia established		Y
	37.68	Abundant charcoal >1mm	Local fire, dry to wet shift	Y
	42.29	Abundant charcoal >1mm	Local fire	Y
	84.3-94.32	Abundant Picea needles	Dry period?	N/N
MIL	20.67	Large decrease in pH		Y
	26.09	S. Acutfolia established		Y
	28.25	Charred Sphagnum	Possible fire	Y
	43.77	Charcoal >1mm, charred macros	Local fire	Y
	48.44	Charcoal >1mm, charred macros	Local fire	N
	61.12-64.08	Charcoal >1mm, charred macros	One/multiple local fires	Y/N
UTK	28.32	Shift to S. Acutfolia; C/N increase		Y
	34.59-42.84		Permafrost possible	Y/Y
	47.01	Charcoal >1mm, charred needles	Local fire	Y
	55.22	Charcoal >1mm, charred needles	Local fire	Y
	72.58	Shift to S. Acutfolia, charcoal >1mm, charred needles	Local fire	N
	86.75-89.53	Charcoal >1mm, charred needles	One/multiple local fires	N/N

Table 2: Average major element geochemical data for identifiable populations of analysed tephra samples and suggested correlations. (#) = standard deviation; FeOt = total iron oxide as FeO; H2Od = water by difference.

a) Samples used as isochrons

Site	Depth (cm)	Sample #	UA #	SiO_2	TiO_2	Al_2O_3	FeO_t	MnO	MgO	CaO	Na_2O	K_2O	Cl	Total	$H2O_d$	n	Correlation
ANZ	37.60	39	2969	77.98	0.15	12.27	1.13	0.05	0.10	0.72	4.15	3.26	0.24	100	1.48	31	Novarupta-Katmai 1912
				(0.23)	(0.04)	(0.13)	(0.04)	(0.03)	(0.01)	(0.03)	(0.23)	(0.08)	(0.09)		(1.38)		
	83.22	83	2919	74.42	0.19	14.15	1.35	0.04	0.32	1.72	3.99	3.46	0.35	100	0.86	19	Mt. Churchill - WRAe
				(0.99)	(0.05)	(0.52)	(0.24)	(0.02)	(0.08)	(0.25)	(0.15)	(0.23)	(0.03)		(1.17)		
JPH	14.86	16	2913	77.71	0.16	12.31	1.17	0.05	0.13	0.81	4.19	3.25	0.23	100	2.55	15	Novarupta-Katmai 1912
				(1.39)	(0.07)	(0.67)	(0.17)	(0.02)	(0.09)	(0.3)	(0.32)	(0.11)	(0.04)		(1.4)		
	53.22	54	2873	74.00	0.20	14.30	1.40	0.05	0.34	1.81	4.07	3.56	0.36	100	1.34	34	Mt. Churchill - WRAe
				(0.87)	(0.05)	(0.47)	(0.18)	(0.02)	(0.09)	(0.19)	(0.24)	(0.19)	(0.03)		(1.51)		
McK	75.83	65	2877	73.88	0.20	14.29	1.46	0.05	0.35	1.71	4.24	3.54	0.35	100	1.21	33	Mt. Churchill - WRAe
				(0.83)	(0.05)	(0.35)	(0.19)	(0.02)	(0.08)	(0.25)	(0.38)	(0.29)	(0.04)		(1.42)		
McM	28.66	26	2968	77.88	0.17	12.33	1.17	0.05	0.11	0.76	4.10	3.27	0.22	100	1.37	30	Novarupta-Katmai 1912
				(0.38)	(0.05)	(0.17)	(0.1)	(0.03)	(0.04)	(0.12)	(0.22)	(0.1)	(0.04)		(1.56)		
	57.49	51	2920	73.76	0.20	14.28	1.44	0.06	0.35	1.53	4.24	3.78	0.36	100	1.16	15	Mt. Churchill - WRAe
				(0.96)	(0.05)	(0.32)	(0.21)	(0.03)	(0.08)	(0.37)	(0.43)	(0.57)	(0.04)		(2.4)		
MIL	34.72	32	2914	78.17	0.15	12.07	1.11	0.04	0.11	0.73	4.17	3.22	0.23	100	0.75	16	Novarupta-Katmai 1912
				(0.25)	(0.03)	(0.16)	(0.04)	(0.02)	(0.01)	(0.02)	(0.24)	(0.12)	(0.03)		(2.46)		
UTK	67.11	65	2924	74.05	0.18	14.25	1.41	0.05	0.34	1.73	4.02	3.63	0.36	100	1.71	18	Mt. Churchill - WRAe
				(1.04)	(0.05)	(0.52)	(0.23)	(0.03)	(0.11)	(0.25)	(0.31)	(0.37)	(0.05)		(1.69)		

b) Other samples analysed

Site	Depth (cm)	Sample #	UA #	SiO_2	TiO_2	Al_2O_3	FeO_t	MnO	MgO	CaO	Na_2O	K_2O	Cl	Total	$H2O_d$	n	Correlation
ANZ	38.62	40	2907	73.80	0.21	14.35	1.49	0.04	0.39	1.81	4.13	3.40	0.37	100	2.21	6	Mt. Churchill
				(0.24)	(0.02)	(0.15)	(0.12)	(0.02)	(0.07)	(0.12)	(0.25)	(0.2)	(0.03)		(1.51)		
				78.05	0.15	12.10	1.13	0.05	0.13	0.72	4.24	3.22	0.21	100	1.58	4	Novarupta-Katmai 1912
				(0.3)	(0.02)	(0.02)	(0.03)	(0.03)	(0.02)	(0.03)	(0.21)	(0.13)	(0.01)		(0.2)		
	40.75	42	2971	76.05	0.38	12.82	2.11	0.05	0.41	2.19	3.58	2.27	0.17	100	1.24	5	Unknown
				(0.92)	(0.05)	(0.27)	(0.26)	(0.01)	(0.08)	(0.26)	(0.25)	(0.14)	(0.03)		(0.55)		
			2908, 2971	74.89	0.18	14.34	1.54	0.05	0.31	1.67	4.54	2.39	0.11	100	1.70	10	Mt. St. Helens ash bed Z
				(0.7)	(0.04)	(0.3)	(0.21)	(0.02)	(0.03)	(0.18)	(0.4)	(0.12)	(0.02)		(0.89)		

Site	Depth (cm)	Sample #	UA #	SiO_2	TiO_2	Al_2O_3	FeO_t	MnO	MgO	CaO	Na_2O	K_2O	Cl	Total	$H2O_d$	n	Correlation
ANZ				(0.38)	(0.08)	(0.36)	(0.08)	(0.02)	(0.03)	(0.1)	(0.32)	(0.02)	(0.02)		(0.63)		
				72.81	0.42	14.59	1.86	0.04	0.46	1.61	5.14	2.90	0.20	100	1.42	5	Unknown
				(0.88)	(0.05)	(0.16)	(0.3)	(0.03)	(0.08)	(0.18)	(0.42)	(0.3)	(0.03)		(0.85)		
	41.82	43	2967	74.20	0.19	14.14	1.63	0.01	0.31	1.44	3.70	4.25	0.17	100	4.05	3	Unknown
				(0.39)	(0.02)	(0.28)	(0.02)	(0.01)	(0.03)	(0.15)	(0.34)	(0.21)	(0.05)		(0.89)		
				76.95	0.04	12.98	0.80	0.10	0.04	0.56	3.73	4.73	0.08	100	5.55	3	Unknown
				(0.53)	(0.02)	(0.27)	(0.29)	(0.08)	(0.03)	(0.02)	(0.15)	(0.3)	(0.01)		(0.2)		
	42.89	44	2909	74.63	0.22	14.18	1.67	0.04	0.33	1.66	4.76	2.40	0.11	100	2.32	5	Mt. St. Helens ash bed Z
				(0.09)	(0.04)	(0.05)	(0.05)	(0)	(0.03)	(0.03)	(0.22)	(0.08)	(0.03)		(1.11)		
McK	41.18	36	2966	73.94	0.28	14.05	1.71	0.03	0.28	1.22	4.03	4.39	0.10	100	1.91	9	Unknown
				(0.28)	(0.06)	(0.13)	(0.06)	(0.03)	(0.01)	(0.04)	(0.29)	(0.09)	(0.01)		(0.72)		
				75.22	0.36	13.65	1.31	0.03	0.31	1.22	4.37	3.41	0.14	100	2.45	5	Unknown
				(0.35)	(0.03)	(0.26)	(0.06)	(0.01)	(0.04)	(0.08)	(0.12)	(0.17)	(0.03)		(1.4)		
				74.10	0.21	14.31	1.44	0.07	0.36	1.67	3.84	3.71	0.37	100	2.48	3	Unknown
				(0.96)	(0.09)	(0.5)	(0.28)	(0.02)	(0.14)	(0.26)	(0.19)	(0.4)	(0.04)		(0.88)		
				75.65	0.07	13.24	1.17	0.04	0.03	0.57	4.25	4.90	0.10	100	3.26	5	Unknown
				(1.2)	(0.02)	(0.54)	(0.16)	(0.03)	(0.02)	(0.09)	(0.18)	(0.3)	(0.02)		(0.99)		
MIL	65.45	57	2922	73.86	0.19	14.20	1.33	0.05	0.33	1.72	3.52	4.43	0.36	100	2.57	8	Mt. Churchill - WRAe
				(0.78)	(0.04)	(0.36)	(0.19)	(0.02)	(0.08)	(0.24)	(0.59)	(1.03)	(0.03)		(1.94)		
				64.60	0.96	15.84	5.54	0.18	1.80	4.30	4.11	2.53	0.15	100	1.28	7	Low SiO2 mix
				(3.84)	(0.22)	(0.32)	(2.14)	(0.03)	(0.91)	(1.63)	(0.9)	(0.53)	(0.04)		(1.19)		
UTK	36.69	36	2970	78.07	0.14	12.29	1.17	0.03	0.10	0.73	3.95	3.32	0.25	100	2.03	3	Novarupta-Katmai 1912
				(0.21)	(0.05)	(0.02)	(0.03)	(0.02)	(0.01)	(0.02)	(0.24)	(0.11)	(0.02)		(0.4)		

c) Reference material analysed concurrently

Site	UA #	SiO_2	TiO_2	Al_2O_3	FeO_t	MnO	MgO	CaO	Na_2O	K_2O	Cl	Total	$H2O_d$	n	Correlation
Carmacks, Yukon Territory	1119	73.55	0.23	14.58	1.50	0.05	0.37	1.80	4.28	3.35	0.34	100	2.68	28	Mt. Churchill - WRAe
		(0.5)	(0.05)	(0.28)	(0.15)	(0.03)	(0.06)	(0.15)	(0.21)		(0.02)		(0.89)		
Kodiak Island, Alaska	1364	74.93	0.37	13.15	2.06	0.06	0.42	1.69	4.23	2.91	0.19	100	1.14	42	Novarupta-Katmai 1912
		(3.41)	(0.21)	(1.13)	(0.96)	(0.03)	(0.36)	(0.99)	(0.25)	(0.31)	(0.03)		(1.3)		(all data)
		78.03	0.15	12.16	1.19	0.05	0.11	0.79	4.15	3.19	0.22	100	1.03	16	Novarupta-Katmai 1912
		(0.26)	(0.04)	(0.18)	(0.06)	(0.02)	(0.03)	(0.09)	(0.23)	(0.1)	(0.02)		(0.85)		(high SiO2 popn only; >77%)
Washington	2310	75.24	0.23	13.90	1.54	0.04	0.27	1.52	4.72	2.46	0.10	100	2.20	21	Mt. St. Helens ash bed Z
		(0.68)	(0.03)	(0.39)	(0.13)	(0.02)	(0.05)	(0.18)	(0.23)	(0.13)	(0.02)		(1.63)		

Table 3: Summary of 14C dates produced from the six peat cores. BC dates are shown in blue italics; starred (*) dates are interpreted as anomolous. 14C dates were calibrated using Bomb13NH1 (Hua et al., 2013) and IntCal13 (Reimer et al., 2013) calibration curves as appropriate in Oxcal v4.2 (Bronk Ramsey, 2009a).

Sample ID	**UCIAMS #**	**Depth (cm)**	**Description**	**F ^{14}C**	**±**	**^{14}C age (BP)**	**±**	**Calibrated age (cal BC/AD)**			
								68.2% range		**95.4% range**	
ANZ-W3 #05	170621	5.99	*Sphagnum* stems	1.0634	0.0017	---	---	2005-2006	---	2005-2008	1956-1957
ANZ-W3 #10	170623	10.62	*Sphagnum* stems	1.0675	0.0019	---	---	2004-2006	---	2003-2007	1956-1957
ANZ-W3 #15	154027	14.98	*Sphagnum* stems	1.1521	0.0023	---	---	1990-1991	---	1957-1958	1989-1991
ANZ-W3 #20	154026	19.20	*Sphagnum* stems	1.2131	0.0022	---	---	1960-1961	1984-1985	1959-1961	1983-1985
ANZ-W3 #25	154025	23.75	*Sphagnum* stems	1.3133	0.0025	---	---	1978-1979	---	1962	1977-1979
ANZ-W3 #30	154024	28.45	*Sphagnum, Ericaceae* leaves	1.4155	0.0025	---	---	1962	1974	1962-1963	1973-1974
ANZ-W3 #40	142039	38.62	Twig material	---	---	170	20	1669-1682; 1736-1780; 1799-1805	1935-1944	1665-1693; 1727-1785; 1793-1813	1919-
ANZ-W3 #50	152367	49.01	*Sphagnum* stems, *Picea* needles	---	---	330	15	1514-1528	1553-1599; 1617-1633	1490-1603	1613-1637
ANZ-W3 #60	142038	59.31	*Sphagnum* stems	---	---	325	20	1516-1530; 1539-1596	1618-1635	1490-1603	1612-1642
ANZ-W3 #70	152362	69.62	*Sphagnum* stems and branches, *Picea* needles, *Chamaedaphne calyculata* seed	---	---	910	15	1049-1085	1124-1137; 1150-1160	1041-1108	1116-1165
ANZ-W3 #80	142043	80.15	*Sphagnum* stems and leaves	---	---	1245	25	689-751	760-775	682-779	790-869
JPH4-W1 #5	154012	4.31	*Sphagnum, Picea* needles	1.2789	0.0023	---	---	1979-1980	---	1959; 1961-1962	1979-1980; 1981
JPH4-W1 #10	154011	9.08	*Sphagnum* stems	1.7993	0.0033	---	---	1965	---	1963-1965	---
JPH4-W1 #14	154009	12.89	*Sphagnum* stems	1.2479	0.0023	---	---	1981-1982	---	1959; 1961-1962	1980-1982
JPH4-W1 #20	154008	18.93	*Sphagnum* stems, *V. oxycoccos* charred leaves, *Picea* charred needles	---	---	95	15	1698-1724	1815-1835; 1878-1395; 1903-1917	1694-1728	1812-1919
JPH4-W1 #30	142066	28.65	*Sphagnum* stems	---	---	490	40	1411-1445	---	1324-1346	1393-1464

Sample ID	UCIAMS #	Depth (cm)	Description	F ^{14}C	±	^{14}C age (BP)	±	Calibrated age (cal BC/AD)			
								68.2% range		95.4% range	
JPH4-W1 #39-40	152359	38.30	*Sphagnum* stems, *Conifer/Ericaceae* bark, *Carex* seeds, *Picea* charred needles	---	---	605	20	1306-1329; 1341-1363	1385-1396	1299-1370	1380-1404
JPH4-W1 #50	142037	49.13	Bark	---	---	955	20	1029-1047	1091-1121; 1140-1148	1022-1059	1069-1155
JPH4-W1 #59	152360	58.47	*Carex* seeds, Conifer bark, *Ericaceae* stems	---	---	1290	15	678-710	746-764	670-723	740-768
JPH4-W1 #70	142045	70.07	Stem and fragments (ligneous)	---	---	2405	20	*448-409*	---	*703-696*	*541-402*
McK-W2 #10	154007	11.76	*Sphagnum* stems	1.1453	0.0025	---	---	1990-1992	---	1957-1958	1990-1992
McK-W2 #15	154006	17.39	*Sphagnum* stems	1.2336	0.0022	---	---	1960	1982-1983	1959-1960; 1961-1962	1982-1983
McK-W2 #20	154005	22.96	*Sphagnum* stems	1.5258	0.0033	---	---	1970	1971	1969-1971	---
McK-W2 #25	154004	28.58	*Sphagnum*, Rhododendron leaves	1.7272	0.0031	---	---	1966	---	1965-1966	---
McK-W2 #40	142064	45.92	*Sphagnum* stems and leaves	---	---	280	20	1528-1551	1634-1651	1521-1576; 1584-1591	1626-1662
McK-W2 #50	152365	57.90	*Picea* charred needles, *Sphagnum* stems	---	---	1135	15	889-901	921-953	882-972	---
McK-W2 #60	142065	69.77	*Sphagnum* stems and leaves	---	---	1220	20	728-737; 768-779	790-829; 838-865	713-744	765-885
McK-W2 #70	152366	82.29	*Picea* charred needles, Ericaceae charred leaves, *Sphagnum* stems	---	---	1575	15	429-436; 446-472	487-498; 505-535	426-538	---
McK-W2 #77	142068	91.60	*Sphagnum* stems and leaves	---	---	1920	45	25-130	---	*21-11*	*2*-216
MCM W3 #05	170644	5.02	*Sphagnum* stems	1.0901	0.0017	---	---	2000-2001	---	1999-2002	1957
McM-W3 #11	170627	11.74	*Sphagnum* stems	1.1318	0.0017	---	---	1993	---	1992-1994	1957-1958
McM-W3 #17	170634	18.48	*Sphagnum* stems	1.1621	0.0017	---	---	1989-1990	---	1988-1990	1957-1958
McM-W3 #23	170629	25.27	*Sphagnum* stems	1.0004	0.0015	0	15	1954-1955	---	1954-1955	1956-1957
MCM W3 #29	170639	32.06	*Sphagnum* stems	0.9881	0.0017	95	15	1698-1724; 1815-1835	1878-1895; 1903-1917	1812-1919	1694-1728
McM-W3 #35	170626	38.83	*Sphagnum* stems	0.9854	0.0015	120	15	1833-1880; 1915-1926	1688-1706; 1720-1730; 1809-1819	1806-1893	1683-1735; 1907-1930

Sample ID	UCIAMS #	Depth (cm)	Description	F ^{14}C	±	^{14}C age (BP)	±	Calibrated age (cal BC/AD)			
								68.2% range		95.4% range	
McM-W3 #38	154002	42.29	Charred *Picea* and *Larix* leaves	---	---	210	20	1655-1670; 1779-1799	1943-	1648-1682; 1739-1744; 1752-1803	1937-
McM-W3 #42	163396	47.02	*Sphagnum* stems and charred *Larix* leaves	---	---	985	15	1018-1039	---	1016-1047	1092-1122;1140-1148
McM-W3 #52	163398	53.96	*Sphagnum* stems	---	---	950	20	1030-1049	1085-1124; 1137-1150	1025-1059	1065-1155
McM-W3 #60	154001	68.03	*Sphagnum stems*	---	---	1220	20	728-737	768-779; 790-829; 838-865	713-744	765-885
McM-W3 #80	154000	91.50	*Larix leaves, Picea leaves*	---	---	1905	15	76-91	99-124	65-130	---
MIL-W1 #10	154023	10.82	*Sphagnum* stems	1.1235	0.0020	---	---	1993-1995	---	1957-1958	1993-1995
MIL-W1 #15	154022	16.24	Sphagnum, Ericaceae leaves	1.1843	0.0021	---	---	1958-1959	1986-1988	1958-1959	1986-1988
MIL-W1 #20	154021	21.78	*Sphagnum* stems	1.3382	0.0024	---	---	1977	---	1976-1977	1978
MIL-W1 #25	154018	27.17	*Sphagnum* stems	1.2256	0.0022	---	---	1959-1960; 1961	1983-1984	1959-1962	1982-1985
MIL-W1 #30	154017	32.56	*Sphagnum* stems	1.0587	0.0021	---	---	2006-2008	2009-2014	1956	2005-2014
MIL-W1 #35	154016	38.10	*Sphagnum* stems	---	---	25	15	1896-1904	---	1891-1907	---
MIL-W1 #40	142040	43.77	Bark of twigs, twig, woody fragments, seeds	---	---	110	20	1694-1710; 1718-1727	1813-1890; 1910-1917	1685-1733	1807-1896; 1903-1928
MIL-W1 #44	152363	48.44	Charred *Picea*, *Larix* needles and Ericaceae leaves	---	---	675	15	1282-1299	1372-1378	1278-1305	1365-1385
*MIL-W1 #50	142041	55.56	Stems	1.3667	0.0029	---	---	1975-1976	---	1974-1976	---
MIL-W1 #50-51	152364	55.56	Coniferous bark (peridermis)	---	---	990	15	1018-1035	---	1012-1045	1095-1121
MIL-W1 #55	152361	62.60	Charred *Picea* needles	---	---	1135	15	889-901	921-953	882-972	---
MIL-W1 #58	142042	66.98	Charcoal particles	---	---	1500	20	551-593	---	478-482	536-620
UTK W2 #05	170646	4.87	*Sphagnum stems*	1.0489	0.0017	---	---	2007-2009	---	2007-2009	1956-1957
UTK W2 #11	170641	11.06	*Sphagnum stems*	1.0846	0.0018	---	---	2001-2002	---	2000-2003	1957
UTK-W2 #17	170630	17.10	*Sphagnum stems*	1.1349	0.0018	---	---	1992-1993	---	1991-1994	1957-1958

Sample ID	UCIAMS #	Depth (cm)	Description	F ^{14}C	±	^{14}C age (BP)	±	Calibrated age (cal BC/AD)			
								68.2% range		95.4% range	
UTK W2 #23	170642	23.18	*Sphagnum stems*	1.2225	0.0021	---	---	1983-1984	1959-1960	1983-1985	1959-1962
UTK-W2 #29	170624	29.36	*Sphagnum stems*	1.3755	0.0023	---	---	1974-1976	---	1974-1976	1962
UTK-W2 #32	163401	32.50	*Sphagnum stems*	1.5449	0.0025	---	---	1969-1970	---	1968-1970	1971
UTK-W2 #42	154015	42.85	*Sphagnum stems*	---	---	55	20	1710-1718	1828-1832; 1890-1910	1697-1725	1814-1835; 1877-1918
UTK-W2 #48	163397	49.07	*Sphagnum stems*	---	---	220	15	1660-1666	1784-1796	1648-1670; 1780-1800	1943-
UTK-W2 #54	163402	55.22	*Sphagnum stems*	---	---	320	15	1522-1530; 1539-1591	1620-1635	1497-1506; 1512-1601	1616-1643
UTK-W2 #62	154014	63.83	*Sphagnum*	---	---	1100	15	901-921	950-980	895-929	939-988
UTK-W2 #84	154013	89.53	*Sphagnum stems*	---	---	2485	15	*594-546*	*648-610; 670-663; 689-681; 754-735*	*696-540*	*721-702; 766-727*

Table 4: Key radiometric parameters associated with each core including the maximum ^{210}Pb activity, the ^{210}Pb and ^{137}Cs inventories, and the mean ^{210}Pb flux.

Site	Unsupported ^{210}Pb								^{137}Cs			^{241}Am peak depth (cm)	Comments
	Maximum activity		Inventory		Flux		Equilibrium depth (cm)	Unsupported ^{210}Pb activity	Inventory		Peak depth (cm)		
	Bq kg^{-1}	±	Bq m^{-2}	±	Bq m^{-2}y^{-1}	±			Bq m^{-2}	±			
ANZ	167	40	3820	73	119	3	40-50	Relatively uniform <20 cm; below this decline is more or less exponential with depth	766	10	1, 18-21, 31.5	35	
JPH	323	21	2340	55	73	2	25	Varied non-monotonically with depth 0-6 cm. Decline more regular in deeper layers; small non-monotonic feature at 18 cm. ^{210}Pb concentrations in dense layers >20 cm close to/below the minimum level of detection	1164	17	*1.5*, *6*, 13	11-13	High values of ^{137}Cs activity in the uppermost layers is unlikely to be a record of atmospheric fallout
McK	361	29	3639	84	113	3	40	Varied non-monotonically with depth 0-30 cm.	1428	18	*1*, *7*, 30	*21*, 29, *36*	High values of ^{137}Cs activity in the uppermost layers is unlikely to be a record of atmospheric fallout
McM	286	27	3307	80	103	3	40	Decline irregular with depth, but no major non-monotonic features Gradient of the decline is significantly steeper >24 cm; lower net peat accumulation rates in the deeper layers Abrupt termination >42 cm may relate to the abrupt change in the nature of the peat at 38 cm	1565	22	17-19, 23	20-27	Small, diffuse peak in ^{241}Am concentrations 20-27 cm implies the secondary ^{137}Cs peak at 23 cm may be a better indicator of the 1963 depth
MIL	233	26	2988	55	93	2	43	Decline more regular Several non-monotonic features that may record brief changes in net peat accumulation	1014	14	24, 31-34	28-34	Two ^{137}Cs peaks are separated by a non-monotonic feature - both features may date from the early 1960s

Site	Unsupported ^{210}Pb								^{137}Cs			^{241}Am peak depth (cm)	Comments
	Maximum activity		Inventory		Flux		Equilibrium depth (cm)	Unsupported ^{210}Pb activity	Inventory		Peak depth (cm		
	Bq kg^{-1}	±	Bq m^{-2}	±	Bq m^{-2}y^{-1}	±			Bq m^{-2}	±			
UTK	285	16	2556	37	80	3	46	0-18 cm: concentrations decline exponentially with depth	820	11	30-34		
								21-33 cm: concentrations constant; separated from the uppermost zone by a small non-monotonic feature,					
								>33 cm: concentrations decline steeply with depth, may be related > peat density here					

Table 5: Comparison of reference dates for AD 1963 (^{137}Cs) and 1912 (cryptotephra) in each core with 210Pb CRS model data. *see also: Table S3b. † No isochron defined.

	1963 depth (cm)		**1912 depth (cm)**		**Reference points used for final age models***
	$^{137}Cs/^{241}Am$	^{210}Pb	Tephra	^{210}Pb	
ANZ	32-37	31.2	37.6	37.8	1963 & 1912
JPH	11-14?	12.5	14.86	19	1912
McK	30	30	None	35.9	None
McM	20-27?	26.3	18.66	37.75	1912
MIL	28-34?	30.15	34.72	40.2	1912
UTK	30-34	34.75	N/A†	40.85	1912

Appendices

A. Peat sub-sampling protocol

Three peat cores were collected from each bog, ca. 3 m apart, using a modified Wardenaar monolith sampler (Wardenaar, 1987). The custom built Ti-Al-Mn alloy corer has serrated cutting edges and removes a monolith of 15 x 15 x 100 cm. The top of the corer is reinforced to allow it to be driven into the bog surface using a nylon sledgehammer: this minimizes compression of the peat core. The peat cores were extracted, photographed, wrapped in polyethylene cling film, then packed into wooden boxes in the field. In the lab, the cores were frozen at -18^{o}C. The living (green) layer at the top of the peat core is removed first: although this material represents the first sample in each peat bog profile, this is living plant material and not peat. The remainder of each core was then cut precisely into 1 cm slices, while frozen, using a stainless steel band saw and polypropylene cutting table.

Each 1cm slice was subsampled as shown in Figure A.1. The edges (1 cm) were trimmed away from each slice and the porewaters extracted for pH and electrical conductivity; these pieces were then dried and combusted to determine ash content and initial tephra counts. A 3 cm slice of each remaining sample was reserved for a separate study of organic contaminants, and a 2 cm wide slice was cut and split for archive material, as well as mercury and macrofossil analyses. Material for ^{14}C analyses was taken from the macrofossil portion, and material tephra geochemical analyses was taken from the archive material. The remaining sample was dried at 105^{o}C for 36 h in polypropylene jars before being ground using a Retsch agate ball mill (PM 400, Haan, Germany) with 250 mL jars containing three 30 mm balls at 300 rpm for four x 2.3 minutes (first forward, then reverse, then forward, then reverse). This portion was used for ^{210}Pb and radioisotope (^{137}Cs, ^{241}Am) analyses.

Figure A.1: Peat subsampling protocol. Tephra counts used material from the trimmed edges; material for tephra geochemical analyses was taken from the archive portion; ^{14}C samples were taken from the macrofossil subsample; ^{210}Pb and radioisotopes were measured on the central oven-dried and milled peat.

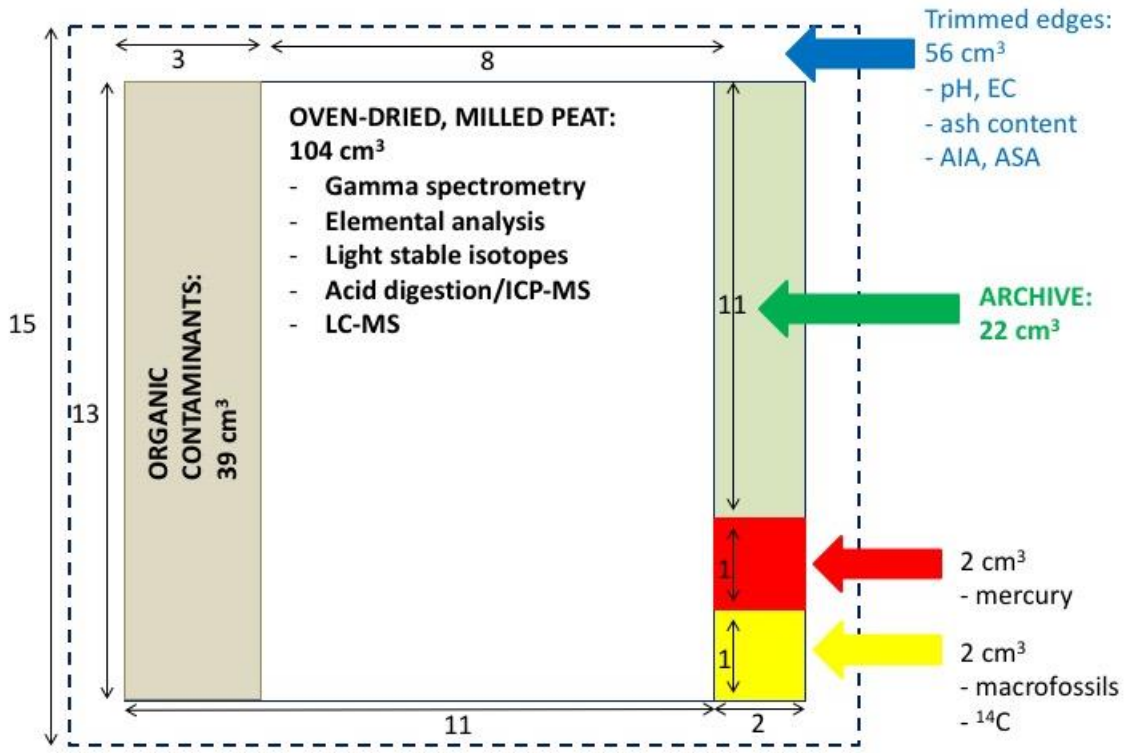

B. ^{210}Pb sample analysis

The sample mass of the dried, milled peat samples used ranged from 1.6-3.5 g (average 2.2 g), depending on peat density. After a 30-day period for equilibration of ^{222}Rn and decay progeny, ^{210}Pb was determined using its gamma-ray emission at 46.5 keV line; ^{226}Ra was determined based on gamma emissions of ingrown decay progeny at 352 (^{214}Pb) and 609 (^{214}Bi) keV; ^{137}Cs and ^{241}Am were determined simultaneously based on their respective photopeaks at 662 and 59.5 keV.

The spectrometers were calibrated for measurement of ^{210}Pb, ^{226}Ra, ^{241}Am, and ^{137}Cs in peat using six, custom-made calibration standards (Eckert and Ziegler Analytics, Atlanta, GA, USA): two low-density (gas-equivalent) standards containing either a nine-nuclide mixture (including ^{137}Cs, ^{241}Am, and ^{210}Pb), or a mixture of ^{210}Pb and ^{226}Ra; and four with the same two radionuclide mixtures homogenously distributed in ancient peat from a Swiss bog spanning the range of densities of the calibration standards (0.02 to 0.41 g/cm^3) All calibration standards are traceable to the National Institute of Standards and Technology (NIST).

Spectra were processed using ORTEC DSPEC Jr. 2.0 Digital Gamma Spectrometer with GammaVision 7 software. Acquisition times of 24, 48, or 72 hours varied depending on the ^{210}Pb activity of the sample. For quality assurance, a check standard of known nuclide activity was measured on each detector between each peat sample. Each successive 1 cm peat slice was measured until ^{210}Pb was observed in equilibrium with its decay-chain parent ^{226}Ra.